

Physiological and morphological development of the rat cerebellar Purkinje cell

Bruce E. McKay and Ray W. Turner

Hotchkiss Brain Institute, University of Calgary, Calgary, Alberta, Canada T2N 4N1

Cerebellar Purkinje cells integrate multimodal afferent inputs and, as the only projection neurones of the cerebellar cortex, are key to the coordination of a variety of motor- and learning-related behaviours. In the neonatal rat the cerebellum is undeveloped, but over the first few postnatal weeks both the structure of the cerebellum and cerebellar-dependent behaviours mature rapidly. Maturation of Purkinje cell physiology is expected to contribute significantly to the development of cerebellar output. However, the ontogeny of the electrophysiological properties of the Purkinje cell and its relationship to maturation of cell morphology is incompletely understood. To address this problem we performed a detailed *in vitro* electrophysiological analysis of the spontaneous and intracellularly evoked intrinsic properties of Purkinje cells obtained from postnatal rats (P0 to P90) using whole-cell patch clamp recordings. Cells were filled with neurobiotin to enable subsequent morphological comparisons. Three stages of physiological and structural development were identified. During the early postnatal period (P0 to ~P9) Purkinje cells were characterized by an immature pattern of Na⁺-spike discharge, and possessed only short multipolar dendrites. This was followed by a period of rapid maturation (from ~P12 to ~P18), consisting of changes in Na⁺-spike discharge, emergence of repetitive bursts of Na⁺ spikes terminated by Ca²⁺ spikes (Ca²⁺-Na⁺ bursts), generation of the trimodal pattern, and a significant expansion of the dendritic tree. During the final stage (> P18 to P90) there were minor refinements of cell output and a plateau in dendritic area. Our results reveal a rapid transition of the Purkinje cell from morphological and physiological immaturity to adult characteristics over a short developmental window, with a close correspondence between changes in cell output and dendritic growth. The development of Purkinje cell intrinsic electrophysiological properties further matches the time course of other measures of cerebellar structural and functional maturation.

(Received 26 April 2005; accepted after revision 3 July 2005; first published online 7 July 2005)

Corresponding author R. W. Turner: Hotchkiss Brain Institute, University of Calgary, 3330 Hospital Dr. N.W., Calgary, Alberta, Canada T2N 4N1. Email: rwturner@ucalgary.ca

The cerebellum underlies the control of posture and balance, fine coordination of motor movement, adaptation of ocular responses, and learning of some conditioned behaviours (Ito, 1984). The expression of each of these behaviours is developmentally regulated in many species. For the rat, cerebellar-dependent behaviours are essentially absent at the time of birth (Altman & Bayer, 1997). A progressive improvement is seen over the first few weeks of life, and by the fourth postnatal week the expression of postural, motoric, ocular and learning-related behaviours reach adult levels. Occurring in parallel with the development of these capacities is a robust anatomical maturation of the cerebellum (Altman & Bayer, 1997). Seen at birth as small, paired masses of tissue overlying the fourth ventricle, the cerebellum rapidly expands, and parcels into distinct lobules. After three postnatal weeks cell migration has completed and adult-like

lamination of the cortex is evident. Neuronal morphology and synaptic connectivity finish developing during the third and fourth postnatal weeks, coincident with the final maturation of cerebellar-dependent behaviours (Crepel, 1971, 1974; Altman, 1972; Puro & Woodward, 1977*a,b*; Stanton *et al.* 1998).

Less well understood is the electrophysiological maturation of cell types within the cerebellum. Of particular interest is the Purkinje cell, as its axons comprise the only output of the cerebellar cortex, and because it expresses ionic conductances that enable sustained and regular spike discharge even in the absence of synaptic input (Ito, 1984; Hausser & Clark, 1997; Nam & Hockberger, 1997; Raman & Bean, 1997). These factors suggest that the electrophysiological development of intrinsic Purkinje cell properties may correlate with the development of the basal output of the cerebellum

as a whole. The time course of maturation of Purkinje cell dendrites is further expected to influence spike output properties, given the prominent dendritic Ca^{2+} spikes that shape somatic Na^{+} -spike discharge (Llinas & Sugimori, 1980b; McKay & Turner, 2004; Womack & Khodakhah, 2004). To date, the developmental characterization of Purkinje cells *in vivo*, and in acute *in vitro* slice preparations has been limited to a few parameters of spontaneous spike output (Woodward *et al.* 1969; Crepel, 1972; Womack & Khodakhah, 2002a), whereas the developmental study of Purkinje cells in culture has been more extensive (Gruol & Franklin, 1987; Hockberger *et al.* 1989). The relationship between electrophysiological development and dendritic growth has not been examined, particularly over the age ranges typically utilized in patch clamp recordings.

To gain a detailed understanding of the developmental changes in Na^{+} -spike and Ca^{2+} - Na^{+} burst output, we performed whole-cell current clamp recordings from synaptically isolated Purkinje cells in acute slices obtained from postnatal rats (P0 to P90). All cells were filled with neurobiotin during recording to enable structure–function comparisons. During the early postnatal period (P0 to ~P9) cell output was limited to an immature pattern of Na^{+} -spike discharge, and morphological development was restricted to the soma. Throughout the subsequent postnatal period (~P12 to ~P18) there was a rapid maturation of Ca^{2+} spike-mediated discharge patterns, which coincided with marked dendritic growth. Over the final postnatal period (> P18 to P90) there were minor changes in cell output properties and only a slow increase in dendritic area. Our results indicate a strong correlation between the ontogeny of dendritic structure and the maturation of cell output, which correspond to the development of cerebellar-dependent behaviours.

Methods

Animals

Sprague-Dawley rats were purchased from Charles River Laboratories (Charles River, Quebec, Canada). Timed-pregnant dams arrived during late gestation and were maintained in standard colony conditions by the Animal Resources Centre. Postnatal day zero (P0) was defined as the day of parturition; subsequent postnatal days (e.g. P3, P6) were defined as the number of full days that had elapsed since parturition. The study used a total of 65 male rats, sampled at 3-day intervals between P0 and P45, and at 15-day intervals between P60 and P90. A higher sampling rate was used early in development, as changes in cell properties increased most rapidly over these intervals. Two to five rats, taken from different litters, were used for each age point. All procedures were completed in accordance with the guidelines established by the Canadian Council on Animal Care.

Solutions

Chemicals were obtained from Sigma (St Louis, MO, USA) unless otherwise stated. All procedures have been previously described in detail (McKay *et al.* 2005). Briefly, tissue slicing and electrophysiological recordings were completed with artificial cerebrospinal fluid (aCSF) of the following composition (mM): NaCl 125; KCl 3.25; CaCl_2 1.5; MgCl_2 1.5; NaHCO_3 25; and D-glucose 25. The aCSF was continuously bubbled with carbogen (95% O_2 and 5% CO_2) gas. To study the intrinsic firing properties of Purkinje cells, blockers of inhibitory and excitatory neurotransmission were added to the recording aCSF (μM): picrotoxin 50; (2S)-3-[[[(1S)-1-(3,4-dichlorophenyl)ethyl]amino]-2-hydroxypropyl](phenylmethyl)phosphinic acid (CGP 55845; Tocris, Ellisville, MO, USA) 1; DL-2-amino-5-phosphonopentanoic acid (DL-AP5) 25; and 6,7-dinitroquinoxaline-2,3-dione (DNQX; Tocris) 10. The pipette solution consisted of (mM): potassium gluconate 130; EGTA 0.1; Hepes 10; NaCl 7; MgCl_2 0.3; pH 7.3 with KOH (theoretical junction potential ~11.6 mV). Di-tris-creatine phosphate (5 mM), Tris-ATP (2 mM) and Na-GTP (0.5 mM) were added daily from frozen stock solutions. The syringe containing the electrolyte was maintained at 4°C throughout each experiment. The extracellular and intracellular solutions closely approximate physiological ionic equilibrium potentials at 35°C: $E_{\text{Na}} = 56$ mV; $E_{\text{K}} = -97$ mV; $E_{\text{Cl}} = -76$ mV. Neurobiotin (0.1%; Vector Laboratories, Burlingame, CA, USA) was added to the patch pipette solution to enable visualization of Purkinje cell morphology during subsequent histological processing.

Preparation of tissue slices

Male rat pups and adults were anaesthetized with a single subcutaneous injection of sodium pentobarbital (65 mg kg⁻¹; MTC Pharmaceuticals, Cambridge, ON, Canada). After establishing that a sufficient depth of anaesthesia was reached (e.g. no overt responses to tail or foot pinch) the rat was decapitated, the posterior skull removed, and the cerebellum dissected out and immediately bathed in ice-cold aCSF. The cerebellum was blocked in the sagittal plane by removing one cerebellar hemisphere with a scalpel cut, and then mounted with cyanoacrylate glue on an ice-cold Vibratome cutting tray (Ted Pella, Redding, CA, USA). Sagittal slices (300 μm) were obtained from the cerebellar vermis in carbogen-bubbled ice-cold aCSF. Following cutting, slices were incubated at 35°C for 30–45 min, and subsequently maintained at room temperature (~22°C) for no more than an additional 4 h.

Electrophysiology

Slices were transferred to the heated (35°C) recording chamber on the stage of a Zeiss Axioskop FS-2 microscope and kept in place with a nylon-strung platinum harp. The tissue was continuously perfused with aCSF at $\sim 3 \text{ ml min}^{-1}$. Purkinje cells were visualized with differential interference contrast – infrared (DIC-IR) optics and a Dage MTI Newvicon camera (Michigan City, IN, USA) linked to a video monitor (Hitachi VM9012U) (Stuart *et al.* 1993). Juvenile Purkinje cells (P0 to \sim P9) were identified by their comparatively large somata relative to neighbouring cell types and their intermediate position between the internal and external granule cell layers. Adult Purkinje cells were identified by their characteristic morphology and position within the cortex. The identity of most cells (223 out of 281, see below) was later confirmed on the basis of their morphology as revealed with neurobiotin; the identity of the remainder were confirmed by a comparison of their physiological profiles to similar-aged Purkinje cells. To ensure a diverse sample of Purkinje cells, we did not restrict our recordings to specific lobules or regions within lobules.

Current clamp recordings were obtained with an Axoclamp 2A amplifier in Bridge mode (Axon Instruments, Union City, CA, USA). Dendritic recordings were obtained with an Axopatch 200B amplifier in fast current clamp mode. Data was collected with pCLAMP 8.1 software (Axon Instruments) and was acquired at 25 kHz and low-pass filtered at 10 kHz. Pipettes were pulled from thick-walled (fibre-filled) borosilicate glass (1.5 mm o.d.; A-M Systems, Carlsborg, WA, USA) with a Sutter P-87 puller (Sutter, Novato, CA, USA) and had resistances of 4–8 M Ω . Average series resistance was $12.8 \pm 0.3 \text{ M}\Omega$ ($n = 281$), and was compensated with the bridge balance circuitry. Cells were not analysed if the series resistance changed appreciably during the recording. To measure intracellularly evoked responses, all cells were maintained at -70 mV with hyperpolarizing current. The size of successive current steps to elicit spike discharge and determine frequency–current ($F-I$) relations was based on input resistance: for P3 and P6 the step size was 0.01 nA, for P9, 0.01 or 0.02 nA (depending on the input resistance group), for P12, 0.05 nA, and for \geq P15, 0.1 nA. Local applications of 100 nM TTX, or TTX together with 1 mM Ni^{2+} and 200 μM Cd^{2+} was completed with a system of two pressure electrodes as previously described (McKay & Turner, 2004).

Purkinje cell morphology and imaging

Whole-cell recordings were maintained for at least 10 min to ensure a complete wash-in of the neurobiotin tracer into the Purkinje cell. Following recording, slices were transferred to 4% paraformaldehyde and fixed for several

days at 4°C. Slices were washed in 0.1 M phosphate buffer (PB) for several hours, and then placed in a solution of PB, Triton X-100 (0.1%) and streptavidin-Cy3 (1:1500) and kept in the dark. Slices were gently agitated for several hours to ensure thorough exposure to the streptavidin-Cy3 and then left overnight at 4°C. Slices were washed in PB, mounted on poly D-lysine gel-coated slides, cover-slipped with antifade medium (90% glycerol–PB–0.1% p-phenylenediamine; pH 10), sealed with nail polish, and stored at -20°C . Purkinje cells were imaged on an Olympus FV300 BX50 confocal microscope with FluoView software. Laser intensity was set high enough to resolve individual spines. Images were acquired with a step size (z -axis) of $0.5 \mu\text{m}$ at a resolution of 1024×1024 , and Kalman filtered. To be accepted for our anatomical analyses we required that the cell fill have a high signal-to-noise ratio relative to background fluorescence. To ensure that dendrites had been completely filled with neurobiotin and properly detected with streptavidin-Cy3, we required that dendritic structure be approximately symmetrical along the cell's vertical axis. Further, any cell \geq P21 whose distal dendrites did not penetrate to the surface of the molecular layer was considered incompletely filled (Altman & Bayer, 1997). From these criteria 223 of 281 Purkinje cells were accepted. Before analysis images were collapsed into a two-dimensional projection. The cross-sectional surface areas of the somata and dendrites were measured with the pixel detection feature in Adobe Photoshop (Adobe Systems Inc., San Jose, CA, USA). The maximum width and length of each dendritic tree was also measured. The product of these measures was used to estimate the cross-sectional area of the molecular layer in which the dendrite was located. We then determined the 'dendritic density' by taking the ratio of dendritic surface area relative to the total area of the molecular layer occupied by the dendrite.

Measurements

Data were analysed with Clampfit 9.0 (Axon Instruments) and Origin 7.0 (OriginLab, Northampton, MA, USA). Na^+ -spike properties and the frequency of Na^+ -spike generation were measured with the event detection software in Clampfit 9.0. The voltage threshold of the action potential was measured at the abrupt inflection point between the end of the preceding AHP and the subsequent action potential upstroke. Maximum rate of rise (dV/dt) was measured between the voltage threshold of the action potential upstroke and the peak voltage. This downstroke voltage was subsequently used as the voltage onset of the AHP. For adult Purkinje cells, the end of the AHP was defined as the time of offset of the clearly discernible fast AHP. For juvenile Purkinje cells, which did not express a fast AHP, the end of the AHP coincided with the onset

of the subsequent Na^+ spike (see Fig. 5A–D). Na^+ -spike frequencies were calculated as the inverse of the interspike interval. For Purkinje cells from rats \geq P12, the frequency of the initial burst of Na^+ spikes was calculated over the first 4–5 spikes if a visually apparent boundary between high- and low-frequency discharge was not apparent (e.g. Fig. 3A and B, middle panels), or averaged for all spikes between the first spike of the burst and the last spike preceding the discernible transition to low-frequency discharge (e.g. Fig. 3A and B, right panels). For adult Purkinje cells Na^+ -spike frequencies are the average of all Na^+ spikes in a train (e.g. Fig. 3C and D, middle panels) or the average of the Na^+ spikes preceding the onset of Ca^{2+} - Na^+ bursts (e.g. Fig. 3C and D, right panels). Na^+ -spike frequency for Ca^{2+} - Na^+ bursts is the average frequency of all Na^+ spikes within the Ca^{2+} - Na^+ burst. Ca^{2+} - Na^+ burst duration was measured as the time between the onset voltage of the upstroke of the first Na^+ spike in the burst and the corresponding voltage on the downstroke of the terminal Ca^{2+} spike (see Fig. 6A). The difference between this downstroke voltage and the maximal hyperpolarized voltage of the ensuing AHP was used to calculate the size of the burst AHP. Input resistance was determined by a series of hyperpolarizing steps in cells maintained at -70 mV.

The maximum number of Purkinje cells in each age group is: P0: 9, P3: 13, P6: 13, P9: 17, P12: 22, P15: 19, P18: 15, P21: 16, P24: 15, P27: 20, P30: 15, P33: 23, P36: 15, P39: 13, P42: 15, P45: 14, P60: 11, P75: 12, P90: 12. The actual number of cells per age group differed slightly between variables, as not all measurements could be obtained from all cells. The relationship between most morphological or physiological variables and age were sigmoidal and thus were well fitted ($R > 0.95$) with a Boltzmann function of the following form:

$$y = \max + (\min - \max) / (1 + \exp((P - P_{1/2})/k)),$$

where max and min correspond to the y -axis maximum or minimum points for the morphological or physiological variable, P is the postnatal age, $P_{1/2}$ is the postnatal age at which 50% of adult character has been reached, and k is the slope factor of the relationship. The 20–80% range for maturation of a variable was further calculated from the Boltzmann fit.

Statistical analyses were completed with SPSS V.13 (SPSS, Chicago, IL, USA) and consisted of one-way analyses of variance with the Student-Neuman-Keuls *post hoc* test. Criterion for statistical significance was set at $P < 0.05$. Average values in the text and figures represent the mean \pm standard error. Plots were constructed after binning ages in the following manner: P0 to P18, not binned; P22.5 (i.e. P21 + P24); P28.5 (P27 + P30); P34.5 (P33 + P36); P40.5 (P39 + P42); P52.5 (P45 + P60); and P82.5 (P75 + P90). Binning of older age groups and then plotting postnatal age on a non-linear axis was done to

enhance the visibility of those time periods when the greatest changes in cell properties were occurring.

Results

Development of Purkinje cell morphology

The electrophysiological characteristics of 281 Purkinje cells were examined from P0 to P90, and 223 were successfully filled with neurobiotin, processed for histological evaluation, and imaged on a confocal microscope (Fig. 1A). The neurobiotin-filled cells enabled us to identify three stages of Purkinje cell morphological development: a rapid somatic growth period from P0 to \sim P9, a rapid dendritic growth period from $>$ P9 to \sim P18, and a slow dendritic growth period from $>$ P18 to adulthood.

Purkinje cells examined at P0 consisted of small somata with multipolar peri-somatic dendrites that did not exceed $60 \mu\text{m}$ in length (Fig. 1A). Throughout the first developmental interval somatic size progressively increased, approximately tripling in size and attaining adult-like dimensions by P9 (Fig. 1A and B). Dendritic development over this interval was restricted to a retraction of some of the longer processes, resulting in a high density of short peri-somatic dendrites for many P9 cells (Fig. 1A and C–E). Concomitant with the change in somatic size was a \sim 6-fold drop in input resistance, decreasing between P0 and P9 from $1400 \pm 200 \text{ M}\Omega$ ($n = 7$) to $250 \pm 24 \text{ M}\Omega$ ($n = 17$; $P < 0.01$) (Fig. 1G). Notably, the cross-sectional areas of Purkinje cell somata in our study (Fig. 1B) were similar to the values calculated from a previous histological study (Addison, 1911). This comparison suggests that Purkinje cell morphology was not measurably altered by the whole-cell patch configuration.

During the transition between the first and second developmental stages (i.e. between \sim P9 and \sim P12) significant heterogeneity in Purkinje cell morphology was noted, even within the same animal (Fig. 1A). At P9, 4 of 11 cells had a multipolar peri-somatic dendritic configuration, whereas 7 of 11 cells had developed a single prominent primary stem dendrite (Fig. 1A). Although these two morphological groups could be distinguished on the basis of input resistance: $331 \pm 41 \text{ M}\Omega$ for cells with the immature phenotype, and $175 \pm 19 \text{ M}\Omega$ for cells with the primary dendritic stem morphology ($P < 0.01$), the surface areas of their dendrites did not differ significantly. Previous anatomical work has revealed that Purkinje cells within lobules I, II, IX and X, and those at the base of the primary fissure develop more rapidly than Purkinje cells in other lobules (Altman, 1969; Goodlett *et al.* 1990). Purkinje cells in the early maturing lobules begin outgrowth of a primary dendrite at \sim P6, whereas Purkinje cells in the later maturing lobules begin outgrowth of a primary dendrite \sim 4 days later. Once

initiated, the rate of dendritic growth appears similar between lobules. A comparison of Purkinje cells between lobules at P9 revealed cells with the multipolar dendrite configuration or the more developed primary stem

dendrite configuration in both early and late maturing regions of the cerebellum.

Two populations of Purkinje cells were also seen at P12 (Fig. 1A). One group showed similarities to the mature

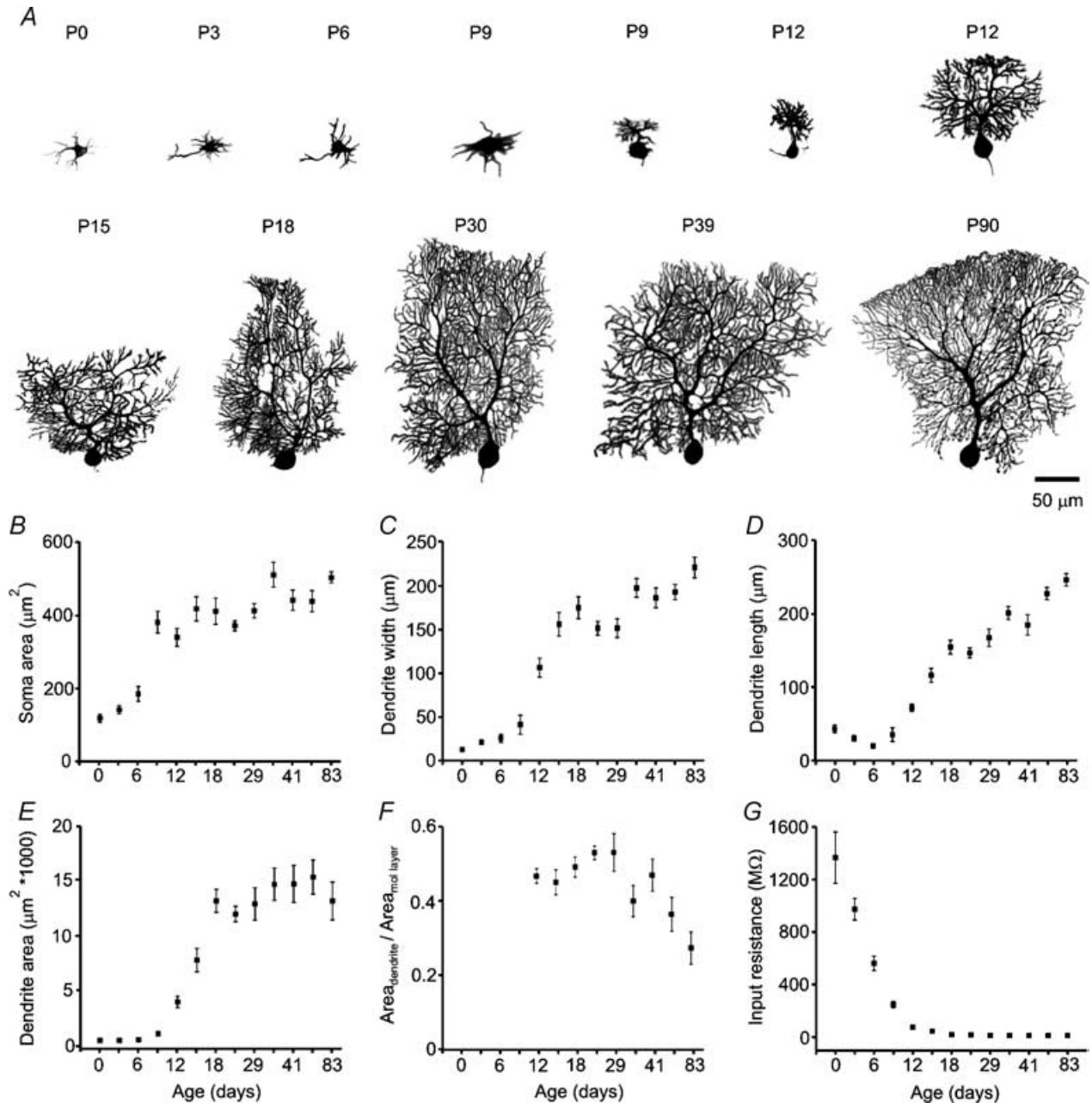


Figure 1. Morphological maturation of the Purkinje cell

A, Purkinje cells matured slowly from P0 to P9, underwent rapid dendritic growth between P12 and P18, and gradually completed development by P90. Note the significant heterogeneity in Purkinje cell morphology at P9 and P12 (two examples at each age illustrated). B, cross-sectional area of the soma matured rapidly between P0 and P9, with little increase in size later in development. C and D, dendritic width (C) and length (D) increased rapidly between P9 and P18, with further increases into adulthood. E, cross-sectional surface area of the dendrites matured rapidly with an asymptote after P18. F, the density of Purkinje cell dendrites within the molecular layer, calculated as the ratio of dendritic surface area to the total cross-sectional area of the molecular layer occupied by the dendrite, decreased after P30. G, Purkinje cell input resistance decreased dramatically over the first 15 postnatal days and reached adult levels by P18. Purkinje cells per data point: in B, 7–26; C, 7–24; D, 7–25; E, 7–24; F, 13–22; and G, 7–31.

(small primary stem dendrite) P9 cells (8 of 19; dendritic area $< 3000 \mu\text{m}^2$), whereas a second group had more robust dendritic development (11 of 19; dendritic area $> 3000 \mu\text{m}^2$). Based on this grouping the dendritic surface areas were $1490 \pm 250 \mu\text{m}^2$ for the immature P12 cells, and $5480 \pm 425 \mu\text{m}^2$ for the mature P12 cells ($P < 0.01$). These groups could also be divided on the basis of input resistance: $111 \pm 23 \text{ M}\Omega$ for the relatively immature group and $58 \pm 6 \text{ M}\Omega$ for the mature group ($P < 0.05$). Again, we found that Purkinje cells with differing degrees of anatomical maturity were not systematically restricted to early or late maturing regions of the cerebellum. Such developmental heterogeneity was not seen before P9 or again after P12, suggesting a distinct transition in dendritic polarity at this time period.

The most conspicuous feature of Purkinje cell development between P9 and P18 was an increase in dendritic size and complexity (Fig. 1A and C–E). Purkinje cells underwent a ~ 4 -fold increase in maximal dendritic width over this interval, from $40 \pm 11 \mu\text{m}$ at P9 ($n = 11$) to $175 \pm 13 \mu\text{m}$ at P18 ($n = 13$) ($P < 0.01$) (Fig. 1C). The maximal length of the dendritic arbour also increased significantly, from $35 \pm 9 \mu\text{m}$ at P9 to $155 \pm 10 \mu\text{m}$ at P18 ($P < 0.01$) (Fig. 1D). This was correlated with a marked increase in dendritic surface area, which reached $13\,000 \pm 1050 \mu\text{m}^2$ by P18 (Fig. 1E).

Over the final developmental period, which extended beyond P18, both the maximal width and length of the dendrites continued to mature significantly, increasing to final adult (P75 to P90) values of $220 \pm 12 \mu\text{m}$ (width) and $250 \pm 8 \mu\text{m}$ (height) ($n = 22$) (Fig. 1C and D). Compared to the cross-sectional area of the molecular layer occupied by each Purkinje cell dendrite at P18 ($\sim 30\,000 \mu\text{m}^2$), the increase in dendritic width and length resulted in a ~ 2 -fold increase in the total area of the molecular layer occupied by the dendrite by P75–90 ($\sim 50\,000 \mu\text{m}^2$). Interestingly, dendritic surface area remained constant over this interval, despite the increase in cell dimensions (Fig. 1C–E), suggesting that the dendrite extends over this interval without a concomitant addition of membrane area. This resulted in a decrease in the density of dendrites per unit area of molecular layer, from $\sim 50\%$ of the total molecular layer area at P30 to $\sim 25\%$ at P90 ($P < 0.05$) (Fig. 1F). Note that Fig. 1F is only plotted for ages \geq P12, as prior to this age the Purkinje cell dendrite is not polarized, and thus an estimate of the proportion of the area of the molecular layer occupied by the dendrite is not valid. Input resistance was stable over this entire interval at $16 \pm 1 \text{ M}\Omega$ (Fig. 1G).

For the cells from mature (\geq P21) rats, we further analysed the anatomical variables as a function of lobule, position within each lobule, and early *vs.* late maturing cerebellar regions. The number of cells from each lobule was: I, 0; II, 9; III, 20; IV, 22; V, 18; VI, 11; VII, 10; VIII, 28; IX, 12; and X, 10. The number of cells from the outer, middle and inner 1/3 of all lobules was 24,

71 and 28, respectively (this parameter not recorded for all cells). The number of cells in the early maturing region was 35 and in the late maturing region was 105. There were no statistically significant differences between lobules, positions within lobules, or cerebellar regions for any of the anatomical variables. Although we did not find developmental differences in morphology between early and late maturing lobules, as has been previously reported (Altman, 1969; Goodlett *et al.* 1990), this may potentially reflect the comparatively small sample sizes used in the present study.

Our data thus revealed three key time-frames for Purkinje cell development: an interval between P0 and \sim P9 in which there was marked somatic growth but minimal dendritic development, an interval from $>$ P9 to \sim P18 when there was minimal somatic change but a marked proliferation of the dendrites, and an interval after P18 characterized by a slow maturation of dendritic dimensions. It will be shown below that these three stages of morphological development correlated with the stages of physiological maturation. Plots of morphological data *vs.* age were well fitted with a Boltzmann function (Table 1), which facilitated this comparison.

Ionic basis of spike discharge

In their pioneering studies on the physiology of cerebellar Purkinje cells, Llinas & Sugimori (1980*a,b*) determined that the large-amplitude, fast-rising and narrow half-width spikes recorded at the soma were due to a Na^+ conductance, and that the lower amplitude, slower rising and broader spikes were due to Ca^{2+} conductances localized in dendrites. To confirm the ionic basis of presumed Na^+ and Ca^{2+} spikes in both juvenile and mature Purkinje cells, we applied 100 nM TTX to block the generation of Na^+ spikes, and then applied a combination of 100 nM TTX, 1 mM Ni^{2+} and 200 μM Cd^{2+} to additionally block Ca^{2+} spikes (Fig. 2A and B). Cells were recorded from the soma and maintained at -70 mV with hyperpolarizing current, and then stimulated with depolarizing current to evoke spiking (Fig. 2A and B). In 10 of 10 Purkinje cells between P4 and P6, TTX abolished all large-amplitude, fast rising events with narrow half-widths, confirming their identity as Na^+ spikes. In these immature cells, TTX application uncovered a single smaller amplitude and slower rising broad depolarization that was eliminated by Ca^{2+} -channel blockers (Fig. 2A). There was no evidence for repetitive Ca^{2+} -spike discharge in the juvenile cells. In 6 of 6 P18 Purkinje cells all large fast spikes were blocked by TTX, identifying these events as Na^+ spikes (Fig. 2B). In contrast to the juvenile cells, application of TTX to more mature cells uncovered a series of repetitive smaller amplitude and slower rising spikes with broader half-widths, which were also abolished by the Ca^{2+} -channel blockers (Fig. 2B).

Table 1. Boltzmann fit parameters for morphological and physiological variables vs. age

Variable	$P_{1/2}$	k	20–80% maturation (P)
Morphology			
Soma			
Length of short axis	6.4	3.4	1.7–11.2
Length of long axis	8.0	2.0	5.3–10.7
Surface area	7.8	2.4	4.5–11.1
Mean	7.4	2.6	3.8–11.0
Dendrite			
Maximum width	11.7	2.5	8.3–15.1
Maximum height	18.8	7.0	9.1–28.4
Surface area	14.1	1.7	11.7–16.5
Total molecular layer area	22.4	4.0	16.9–28.0
Mean	16.8	3.8	11.5–22.0
Physiology			
Na ⁺ -spike output			
Rheobase current	15.4	3.5	10.6–20.2
Minimum Na ⁺ spike Hz	15.3	0.9	14.1–16.6
Threshold voltage	12.5	2.6	8.9–16.2
Maximum rise rate	12.5	1.5	10.5–14.5
Na ⁺ -spike amplitude	14.1	1.0	12.7–15.4
Maximum repolarization rate	13.7	2.3	10.5–16.9
AHP area	11.9	0.9	10.6–13.3
Tonic Na ⁺ spike Hz	15.7	1.6	13.5–17.9
Mean	13.9	1.8	11.4–16.4
Ca ²⁺ -Na ⁺ burst output			
Burst threshold (current)	16.4	1.3	14.5–18.2
Na ⁺ spikes per burst	15.7	0.6	14.8–16.5
Intraburst frequency (Hz)	16.3	1.5	14.2–18.3
Proportion of trimodal cells	17.4	2.5	13.9–20.9
Mean	16.5	1.5	14.4–18.5
Proportion of trimodal cells*	13.4	1.6	11.2–15.6]

All fits were $R > 0.95$, $P < 0.01$. *Boltzmann fit to mouse data from Fig. 3a of Womack & Khodakhah (2002a). P is the postnatal age; k is the Boltzmann function slope factor.

From these experiments we concluded that all large-amplitude, fast rising and narrow half-width spikes were Na⁺-mediated in both juvenile and mature cells. We further concluded that the smaller amplitude, slower rising and broader half-width spikes associated with the early transient burst of Na⁺ spikes in juvenile cells, or that terminated repetitive bursts of Na⁺ spikes in more mature cells, were Ca²⁺-mediated, as supported by previous work (Llinas & Sugimori, 1980a,b; Liljelund *et al.* 2000). We thus used these marked differences in spike characteristics to distinguish Na⁺ from Ca²⁺ spikes in subsequent experiments in the absence of pharmacological manipulations. Further, it proves impractical to study Na⁺- and Ca²⁺-mediated events in isolation of one another. For instance, the Na⁺-spike waveform and the frequency of Na⁺-spike output are partially determined by Ca²⁺-activated K⁺ channels (Raman &

Bean, 1999; Edgerton & Reinhart, 2003; McKay & Turner, 2004; Womack *et al.* 2004). Thus, the characteristics of Na⁺ spikes are significantly altered in the presence of Ca²⁺-channel blockers. Additionally, the frequency of Ca²⁺-spike generation is increased significantly in the presence of Na⁺-channel blockers (Womack & Khodakhah, 2004; McKay *et al.* 2005).

Maturation of $F-I$ relations

The frequency of Na⁺-spike discharge reflects the intensity of depolarization. In Purkinje cells the Na⁺-spike frequency determines the characteristics of the post-synaptic responses in deep cerebellar neurones (Telgkamp *et al.* 2004; McKay *et al.* 2005). Thus, it is important to understand how Na⁺-spike frequency varies as a function of stimulus size. Given the increase in the number of synapses across development (Altman & Bayer, 1997), it is also important to understand the extent to which frequency–stimulus relationships change as the cell matures. To address this issue we held cells at -70 mV with hyperpolarizing current injection, and generated $F-I$ relations for Na⁺ spikes using 3-s-long current steps of finely graded intensity. Current injections were stopped when the stimulus intensity was sufficient to result in spike failure. Most Purkinje cells at P0 (7 of 9) were quiet at rest (-34 ± 3 mV) and could not be induced to fire Na⁺ spikes, even following a hyperpolarizing prestep. The remaining P0 cells had characteristics similar to P3 Purkinje cells, but will not be further discussed.

From P3 to P9, depolarizing current injections uncovered a biphasic $F-I$ relationship for Na⁺-spike generation (Fig. 3A and B). The rheobase current required to evoke Na⁺ spikes increased significantly with age (Fig. 4A and Table 1). With low-intensity current injection, P3 cells transiently discharged higher frequency Na⁺ spikes early in the step, with a strong accommodation in spike frequency for subsequent spikes (Fig. 3A; strong accommodation is most evident after ~ 1 s and is not illustrated). With higher intensity current injection, P3 cells responded with a clearly discernible high-frequency burst of spikes and a rapid return to low-frequency Na⁺-spike discharge (Fig. 3A). By P9 the frequency of Na⁺-spike discharge did not differ between the early and late periods for low-intensity current injection (Fig. 3B). However, with greater current injection a high-frequency burst of Na⁺ spikes was evident initially, followed by a rapid return to low-frequency discharge that was sustained throughout the stimulation (Fig. 3B).

The plot of the $F-I$ relationship for the initial high-frequency burst of Na⁺ spikes revealed an increase in Na⁺-spike frequency as a function of current intensity for P3 to P9 cells (Fig. 3A and B). The gain of the $F-I$ relationship for the early spike burst decreased linearly

with age, from $1030 \pm 220 \text{ Hz nA}^{-1}$ at P3 ($n = 9$) to $276 \pm 37 \text{ Hz nA}^{-1}$ at P9 ($n = 17$) ($P < 0.01$) (Fig. 4B). In contrast to the marked intensity dependence of the early burst of Na^+ spikes, the frequency of post-burst Na^+ spikes was ~ 10 -fold less sensitive to changes in stimulus intensity (Fig. 3A and B; cf. Fig. 4B and C). The gain of the F - I relationship for the sustained low-frequency Na^+ spikes also decreased over this interval ($P < 0.01$) (Fig. 4C).

The two populations of P9 Purkinje cells defined by morphology were not distinguishable physiologically, potentially because the dendritic size for the two populations were similar. At P12, our anatomical data revealed both immature (P9-like) and more mature Purkinje cells (Fig. 1). These anatomical differences at P12 were reflected in two physiological populations. In 10 of 22 P12 cells the immature phenotype persisted, with an early Na^+ -spike burst followed by a series of low-frequency Na^+ spikes similar to the pattern observed at P9. The remaining P12 cells (12 of 22) generated an output similar to cells at \geq P15 (described below). By comparing the input-output relations to cell morphology, we found that 8 of 8 P12 Purkinje cells with P9-like dendritic development (e.g. dendritic area $< 3000 \mu\text{m}^2$) expressed the immature physiological phenotype, whereas cells with more robust

dendritic development could generate Ca^{2+} - Na^+ bursts (11 of 11). Our results thus suggest that a minimum amount of dendritic growth is required to support mature cell output characteristics.

From P15 onwards, low-intensity depolarizing current injection resulted in sustained Na^+ -spike discharge, with no evidence of an early burst of spikes or spike-frequency accommodation later in the current step. However, more intense stimulation resulted in a rapid inactivation of Na^+ spikes and the onset of Ca^{2+} - Na^+ bursts (Fig. 3C and D). To resolve the F - I relations for Na^+ -spike output in cells P15 and older, we considered only those Na^+ spikes that occurred prior to the onset of Ca^{2+} - Na^+ bursts. Compared to younger Purkinje cells (e.g. P9 range ≈ 6 -29 Hz; Fig. 4D and E), the frequency range over which Purkinje cells could now fire was markedly extended. At P15 the threshold frequency of Na^+ -spike discharge was ~ 30 Hz, and spikes did not fail until ~ 250 Hz (Fig. 4D and E). For P18 and older Purkinje cells, Na^+ -spike discharge typically began at ~ 70 Hz, and did not fail until ~ 350 Hz (P18) or until ~ 250 Hz ($> P21$) (Fig. 4D and E). The minimum Na^+ -spike frequency matured by P18 (Fig. 4D), whereas the maximum Na^+ -spike frequency reached adult levels beyond $\sim P27$ (Fig. 4E). The gain of the F - I relationship

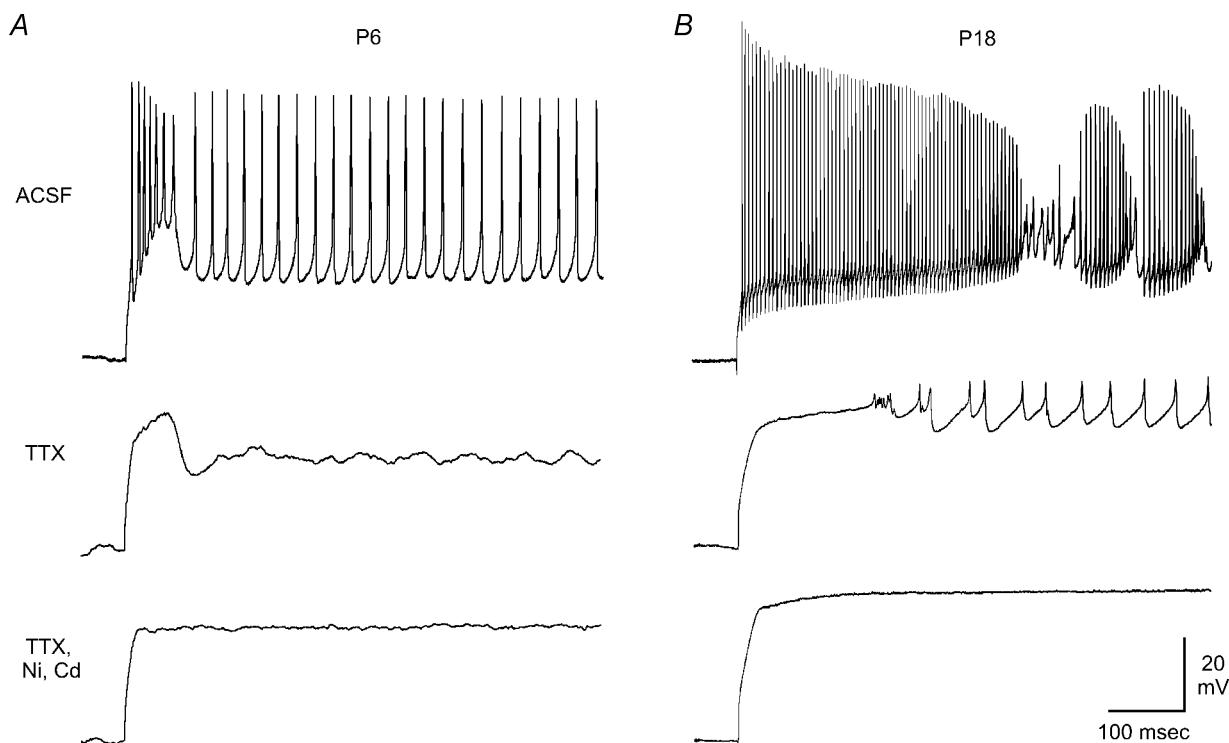


Figure 2. Ionic basis of Purkinje cell spikes

A and B, depolarizing current injections were used to evoke spike discharge in juvenile (P6, A) and more mature (P18, B) Purkinje cells (top panels). Application of the Na^+ -channel blocker TTX eliminated the fast spikes and uncovered a transient membrane depolarization in juvenile cells, and repetitive low-amplitude spikes in more mature cells (middle panels). Subsequent application of the Ca^{2+} -channel blockers Ni^{2+} and Cd^{2+} stopped these slower events (bottom panels).

reached adult levels beyond \sim P33 (Fig. 4C). At these time points both the maximum Na^+ -spike frequency and F - I gain were significantly different from their respective peaks around P18 ($P < 0.01$). There were no statistically significant differences in Purkinje cell input-output relations between cerebellar lobules, nor did

these parameters vary as a function of position within each lobule.

Finally, we calculated the Pearson correlation (r) between stimulus size (current injection) and the Na^+ -spike frequency response across the entire range of stimulus intensities for each cell (Fig. 4F). A correlation of

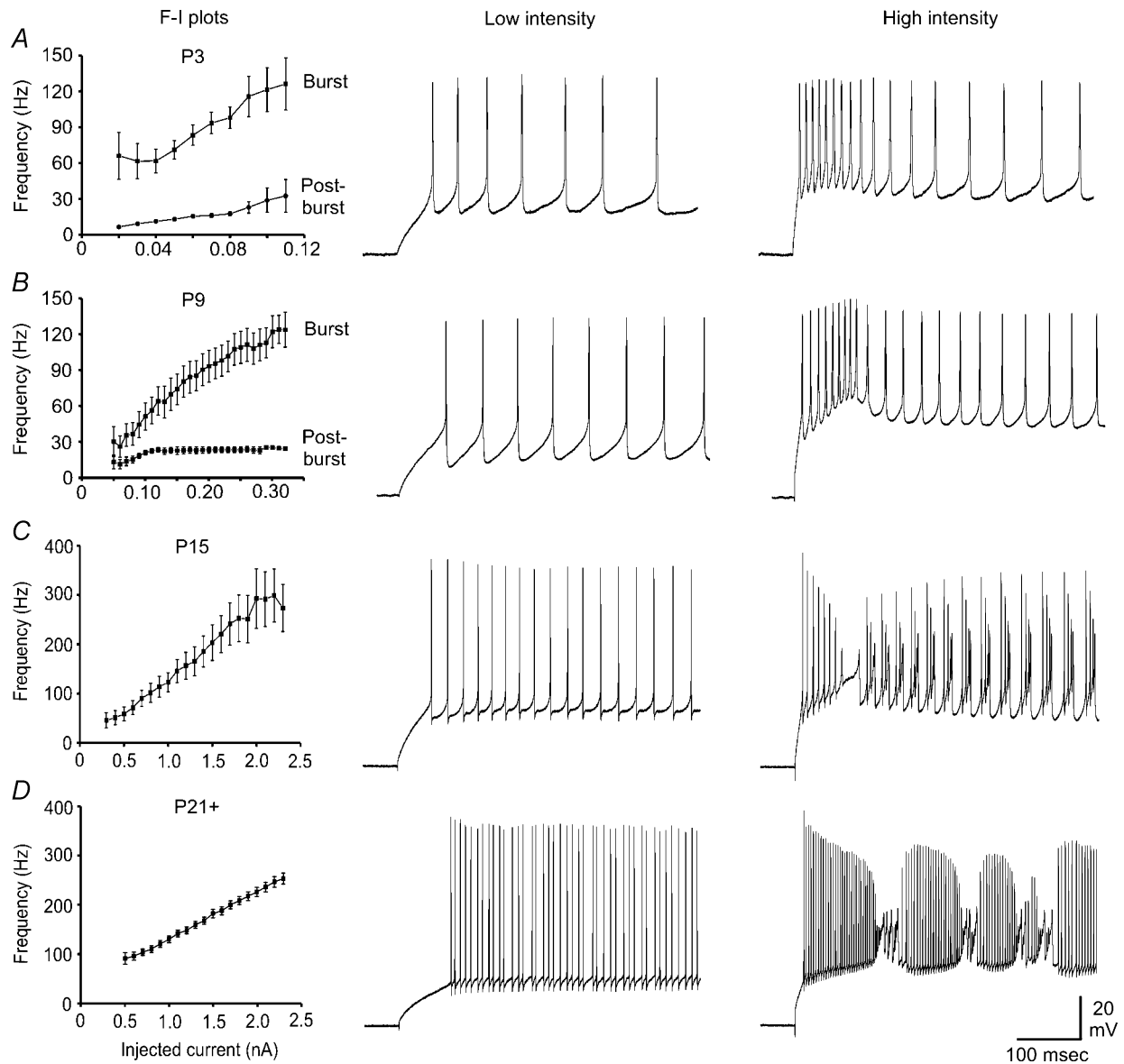


Figure 3. Maturation of Na^+ -spike F - I relations in Purkinje cells

A and B, in response to low-intensity depolarizing current injections Purkinje cells from P3 (A) and P9 (B) rats generated low-frequency Na^+ spikes (middle panels). In response to higher intensity stimulation, these cells generated a brief high-frequency burst of Na^+ spikes followed by a train of low-frequency Na^+ spikes (right panels). The frequency of Na^+ spikes in the early high-frequency burst increased with more intense current injection, whereas the frequency of Na^+ spikes in the postburst period were relatively insensitive to the amount of current injection (left panels). C and D, The frequency of Na^+ spikes in Purkinje cells from P15 rats (C) and P21 or older rats (D) varied linearly as a function of current intensity (left panels). Low intensity depolarizing current injection generated a long train of uninterrupted Na^+ spikes (middle panels). With greater intensity current injection the duration of Na^+ -spike firing was limited, as cells quickly transitioned to a Ca^{2+} - Na^+ burst output mode (right panels). Purkinje cells per data point: in A, 3–9; B, 3–9; C, 7–17; and D, 26–112.

1 across the entire input–output range implies that a given increase in stimulus size will result in a fixed increase in the frequency of Na^+ -spike generation. We found that the correlation between stimulus size and frequency response was as low as 0.49 ± 0.1 for P6 cells, but increased to 0.94 ± 0.01 ($n = 103$) for cells at $\geq \text{P15}$ (Fig. 4F). This result suggests that in mature cells a given stimulus input will result in an almost perfectly predictable increase in the frequency of Na^+ -spike output, but a less predictable output in younger cells. Graded stimulus inputs, such as parallel fibre inputs, are thus expected to result in more precise regulation of spike discharge in mature cells.

In summary, the maturation of Na^+ -spike input–output relations closely paralleled the three stages of anatomical development (Fig. 1). From P3 to $\sim \text{P9}$, when only the somata were maturing in size, Purkinje cells responded to depolarizing current injection with a high-frequency burst of Na^+ spikes, followed by sustained low-frequency Na^+ -spike discharge. From $\sim \text{P12}$ to $\sim \text{P18}$, when Purkinje cells underwent massive dendritic growth, the immature pattern of firing disappeared, the range of possible Na^+ -spike frequencies increased several fold, and at high stimulus intensities Na^+ spikes were inactivated

and Ca^{2+} - Na^+ bursts were evoked. After P18, when the dendrites slowly finished their development, there was a gradual maturation of the input–output relations.

Development of Na^+ -spike characteristics

Na^+ -spike properties, including voltage threshold, amplitude, half-width, and AHP amplitude and duration, all significantly impact synaptic integration. To evaluate how Na^+ -spike characteristics changed across development we measured several spike and AHP parameters. Figure 5A–D illustrates the marked changes in Na^+ -spike properties that were observed as Purkinje cells matured. As noted for morphological variables and F – I relations, the maturation of Na^+ -spike characteristics fell into three developmental periods. Maturation of the Na^+ -spike waveform was remarkable, beginning as a broad and low-amplitude event early in development, and maturing to a large-amplitude spike with an extremely narrow half-width.

From P3 to $\sim \text{P9}$ Na^+ -spike amplitude increased minimally, but showed a slight (~ 10 mV) increase ($P < 0.05$) in spike amplitude at P6 that was not reflected in a change in

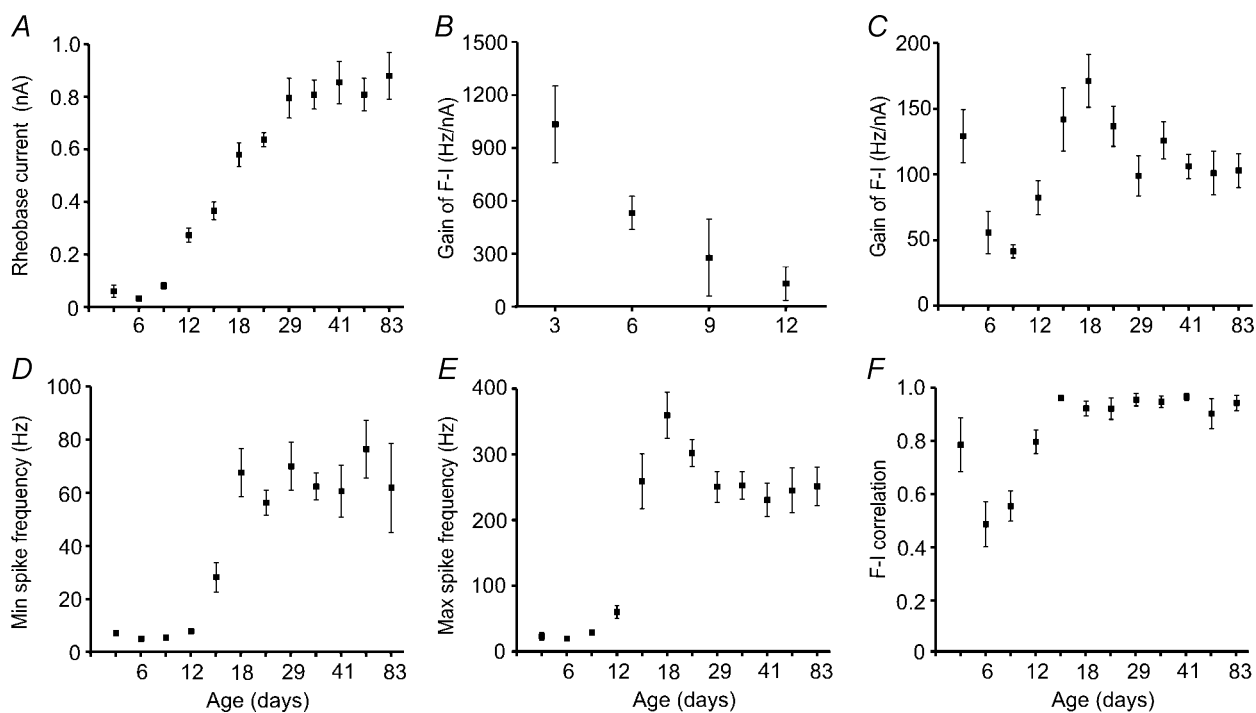


Figure 4. Characteristics of Na^+ -spike F – I relations in Purkinje cells

A, from a membrane potential of -70 mV, the current required to elicit Na^+ spikes increased in a sigmoidal manner with age. B, the gain of the F – I relationship for the transient burst of Na^+ spikes in juvenile cells decreased progressively over the first week of development. C, the gain of the F – I relationship for sustained Na^+ -spike output decreased over the first 9 postnatal days, increased to a maximum around P18, and then matured to lower values. D and E, both the minimum (D) and maximum (E) Na^+ -spike frequencies changed across development. F, the correlation between current intensity and frequency of spike output approached 1 for Purkinje cells $\geq \text{P15}$, conferring a predictable increase in Na^+ -spike frequency for any given increase in stimulus size. Purkinje cells per data point: in A, 10–27; B, 9–17; C, 9–24; D, 10–24; E, 10–24; and F, 7–21.

any other Na⁺-spike parameter (Fig. 5F). The Na⁺-spike half-width decreased substantially from 1.6 ± 0.15 ms ($n = 10$) to 0.75 ± 0.04 ms ($n = 17$; $P < 0.01$) over this interval (Fig. 5G). Interestingly, the maximum amplitude

of the Na⁺-spike AHP increased dramatically between P3 and P9 ($P < 0.01$) (Fig. 5I), but the total area of the AHP did not (Fig. 5J), indicating an acceleration in the rate of onset and decay of the AHP over this age range.

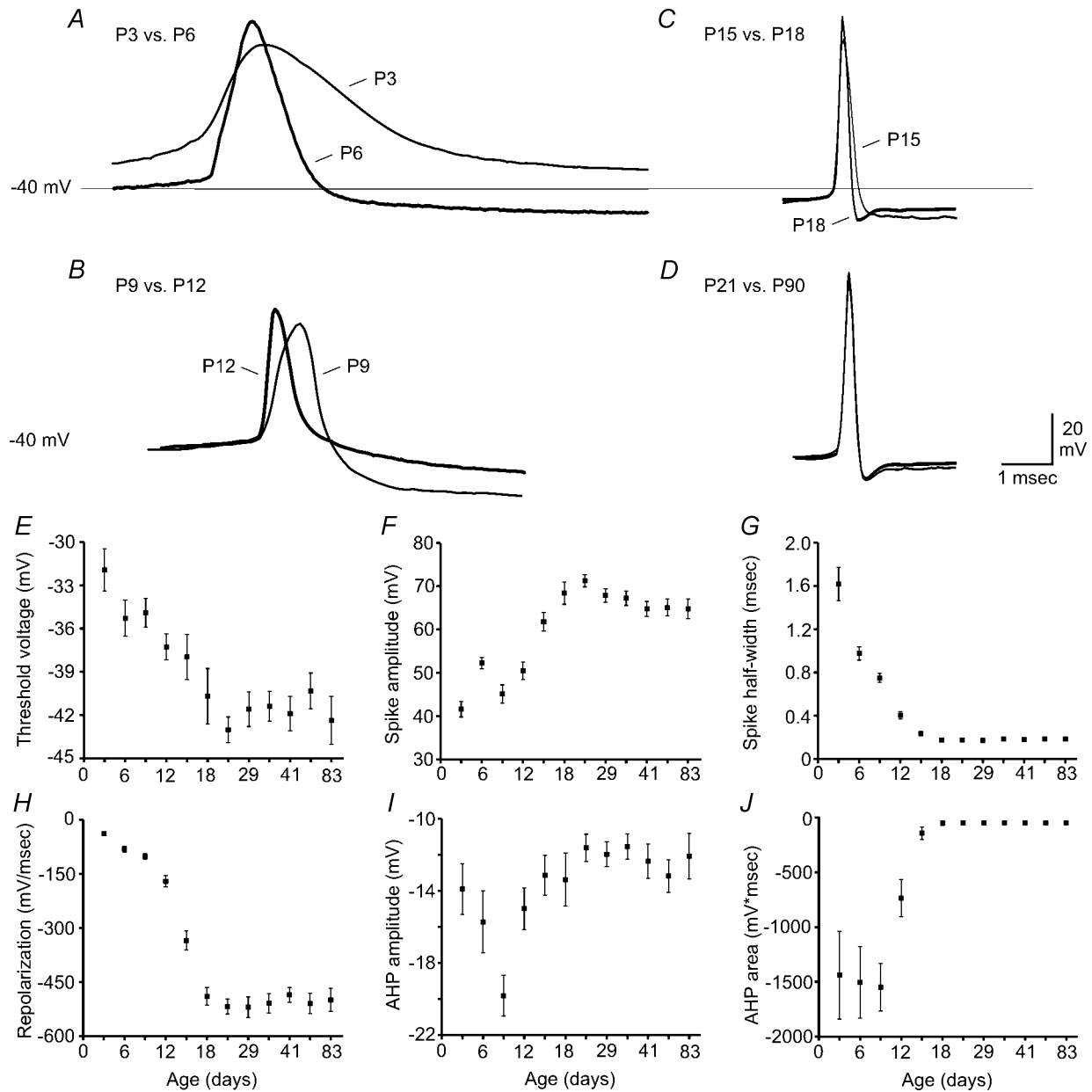


Figure 5. Development of Na⁺-spike properties

A–D, representative single Na⁺ spikes from different ages superimposed for comparison on the same voltage and time scales. A, from P3 (black trace) to P6 (grey trace) Na⁺-spike half-width decreased, amplitude increased, and the threshold for spike activation was reached at lower voltages. B, between P9 (black trace) and P12 (grey trace) Na⁺-spike half-width decreased, amplitude and rate of rise increased, and the AHP became shallower. C, from P15 (black trace) to P18 (grey trace) there was a moderate change in Na⁺-spike half-width and amplitude, and the emergence of a fast AHP. D, no changes were evident in Na⁺-spike characteristics between P21 (black trace) and P90 (grey trace). Horizontal line connecting A and C, and B and D = -40 mV. E, the voltage threshold for Na⁺-spike activation decreased during early development. F–H, the increase in Na⁺-spike amplitude (F) occurred over a similar time frame as the decrease in-spike half-width (G) and the increase in rate of spike repolarization (H). I, from P3 to P9 the amplitude of the Na⁺-spike AHP increased, with a decrease towards adult values over the next several days. J, the Na⁺-spike AHP matured from a slow AHP with large area early in development to a fast AHP with small area later in development. Purkinje cells per data point for E–J, 10–30.

Beginning at \sim P12 and continuing to \sim P18, Na^+ -spike characteristics underwent a marked maturation (Fig. 5B–D and Table 1). By P18 the membrane voltage at which Na^+ spikes were activated shifted (\sim 6 mV hyperpolarized relative to P9; $P < 0.01$; Fig. 5E). Over this interval the peak spike-amplitude increased an additional \sim 18 mV ($P < 0.01$), and half-width decreased substantially from 0.40 ± 0.03 ms (P12; $n = 22$) to the adult value of 0.18 ± 0.01 ms (P18; $n = 15$) ($P < 0.01$; see Fig. 5F and G). A significant ($P < 0.01$) acceleration of spike repolarization was also prominent between P12 and P18 (Fig. 5H). Finally, the Na^+ -spike AHP properties matured to adult levels late in this interval (Fig. 5B–D, I and J). For instance, at P12 only a large-amplitude slow time-course AHP was present, whereas by P18 a fast AHP was prominent. No statistically significant changes in Na^+ -spike or AHP parameters were noted beyond \sim P21 (Fig. 5E–J). Further, Purkinje cell Na^+ -spike characteristics were equivalent across all cerebellar lobules and across the intralobular divisions.

A comparison of the Boltzmann parameters for the Na^+ -spike characteristics and the input–output relations (Table 1) reveal significant temporal parallels between the characteristics of individual Na^+ spikes and cell output characteristics. It is also evident that broad Na^+ spikes with slow AHPs are restricted to Purkinje cells with limited anatomical development, whereas the narrowing of Na^+ spikes and the expression of progressively more distinct fast AHPs occurs concurrently with the elaboration of dendritic structure. As the dendrites themselves are not expected to contribute significantly to individual axonally generated Na^+ spikes *per se*, this structure–function correlation suggests a robust change in the types and distributions of ion channels along the soma–dendritic axis occurring in parallel with the maturation of cell morphology.

Development of Ca^{2+} – Na^+ burst output

In response to low-amplitude depolarizing current injection Purkinje cells generate trains of Na^+ spikes. However, in response to larger amplitude stimuli, Na^+ spikes inactivate rapidly and the Purkinje cell shifts into a Ca^{2+} – Na^+ burst output mode (Llinas & Sugimori, 1980a,b; Edgerton & Reinhart, 2003; McKay & Turner, 2004). Each burst consists of a series of fast Na^+ spikes terminated by a Ca^{2+} spike (Llinas & Sugimori, 1980a,b; Tank *et al.* 1988; McKay & Turner, 2004; Womack & Khodakhah, 2004). In support of the dendritic origin of the terminal Ca^{2+} spike, we found that Ca^{2+} – Na^+ burst firing first appeared in select P12 cells that had developed significant dendritic structure. Maturation of Ca^{2+} – Na^+ burst firing then changed in parallel with further dendritic growth.

The maturation of Ca^{2+} – Na^+ burst firing is illustrated in Fig. 6A. In general, with advancing age came longer duration bursts with intraburst Na^+ spikes generated at higher frequencies and in greater numbers. At P12 (Fig. 6B) and P15 (Fig. 6C) Ca^{2+} – Na^+ burst generation began at a threshold frequency of \sim 10 Hz. With an increase in current injection there was a linear increase in Ca^{2+} – Na^+ burst frequency to a maximum of \sim 25 Hz. Although the range of Ca^{2+} – Na^+ burst frequencies was similar between the two age groups, the gain of the input–output response was significantly higher in P12 cells (16.1 ± 3.1 Hz nA^{-1} ; $n = 9$) compared to P15 cells (8.5 ± 1.6 Hz nA^{-1} ; $n = 16$, $P < 0.05$). At P18 the gain of the Ca^{2+} – Na^+ burst F – I relationship did not differ significantly from that of P15 cells (7.9 ± 1.7 Hz nA^{-1} ; $n = 13$) (Fig. 6D). However, a subtractive effect on the F – I relationship was evident, as the initial Ca^{2+} – Na^+ burst frequency was reduced from 9.2 ± 0.9 Hz at P15 ($n = 16$) to 6.0 ± 0.9 Hz at P18 ($n = 14$; $P < 0.05$), and the peak Ca^{2+} – Na^+ burst frequency was reduced from 22.4 ± 1.6 Hz to 15.9 ± 2.0 Hz ($P < 0.01$) (see Fig. 6C and D). In mature Purkinje cells (e.g. at \geq P21, Fig. 6E) the gain of the burst F – I relationship was only 4.8 ± 1.0 Hz nA^{-1} ($n = 72$).

The time courses of maturation for Purkinje cell structural variables also correlated with the maturation of Ca^{2+} – Na^+ burst output. From P0 to P9 we observed a single burst of Na^+ spikes at the onset of current injection; repetitive bursts of Na^+ spikes terminated by Ca^{2+} spikes (Ca^{2+} – Na^+ bursts) were never observed. Over the interval from P12 to \sim P18, Ca^{2+} – Na^+ bursts occurred in response to progressively larger depolarizations (Fig. 6F and Table 1). The duration of Ca^{2+} – Na^+ bursts, measured from the onset of the first Na^+ spike in the burst to the repolarization of the terminal Ca^{2+} spike, increased over 2-fold from P12 to P18 ($P < 0.01$) (Fig. 6G). Concomitant with a lengthening of individual bursts was a \sim 50% reduction in peak frequency of Ca^{2+} – Na^+ burst output between P15 and adult ($P < 0.01$) (Fig. 6H). A significant reduction in the amplitude of the burst AHP was also noted between P15 and most of the adult ages ($P < 0.01$ to $P = 0.07$) (Fig. 6I). Finally, beyond P15 there was a \sim 5-fold increase in the number of Na^+ spikes within each Ca^{2+} – Na^+ burst ($P < 0.01$) (Fig. 6J). This change, in combination with a smaller increase in the duration of Ca^{2+} – Na^+ bursts over this interval, resulted in a doubling of the intraburst Na^+ -spike frequencies to values of > 200 Hz ($P < 0.01$) (Fig. 6K). No additional changes in Ca^{2+} – Na^+ burst output characteristics were noted beyond \sim P21. The characteristics of Ca^{2+} – Na^+ burst output were homogeneous throughout the cerebellar lobules.

The mean $P_{1/2}$ of the Boltzmann fits for all Ca^{2+} – Na^+ variables (16.5) was equivalent to the mean $P_{1/2}$ for all anatomical variables describing dendritic maturation (16.8) (Table 1). Furthermore, the 20% to 80% maturation of Ca^{2+} – Na^+ variables fell on average

between P14.4 and P18.5, and was encapsulated by the 20% to 80% maturation period for dendritic structure that extended from P11.5 to P22. These calculations suggest that the onset of Ca^{2+} - Na^+ burst output is correlated with the development of some minimum amount of dendritic structure, and highlights the parallel development of repetitive Ca^{2+} -dependent spiking and dendritic maturation.

Maturation of the trimodal pattern

Purkinje cells *in vitro* and *in vivo* express a trimodal pattern of outputs during spontaneous discharge, first identified by Khodakhah and colleagues (Womack & Khodakhah, 2002a; Cerminara & Rawson, 2004; McKay *et al.* 2005). This pattern consists of a train of tonic Na^+ spikes followed by a series of Ca^{2+} - Na^+ bursts and finally a quiescent

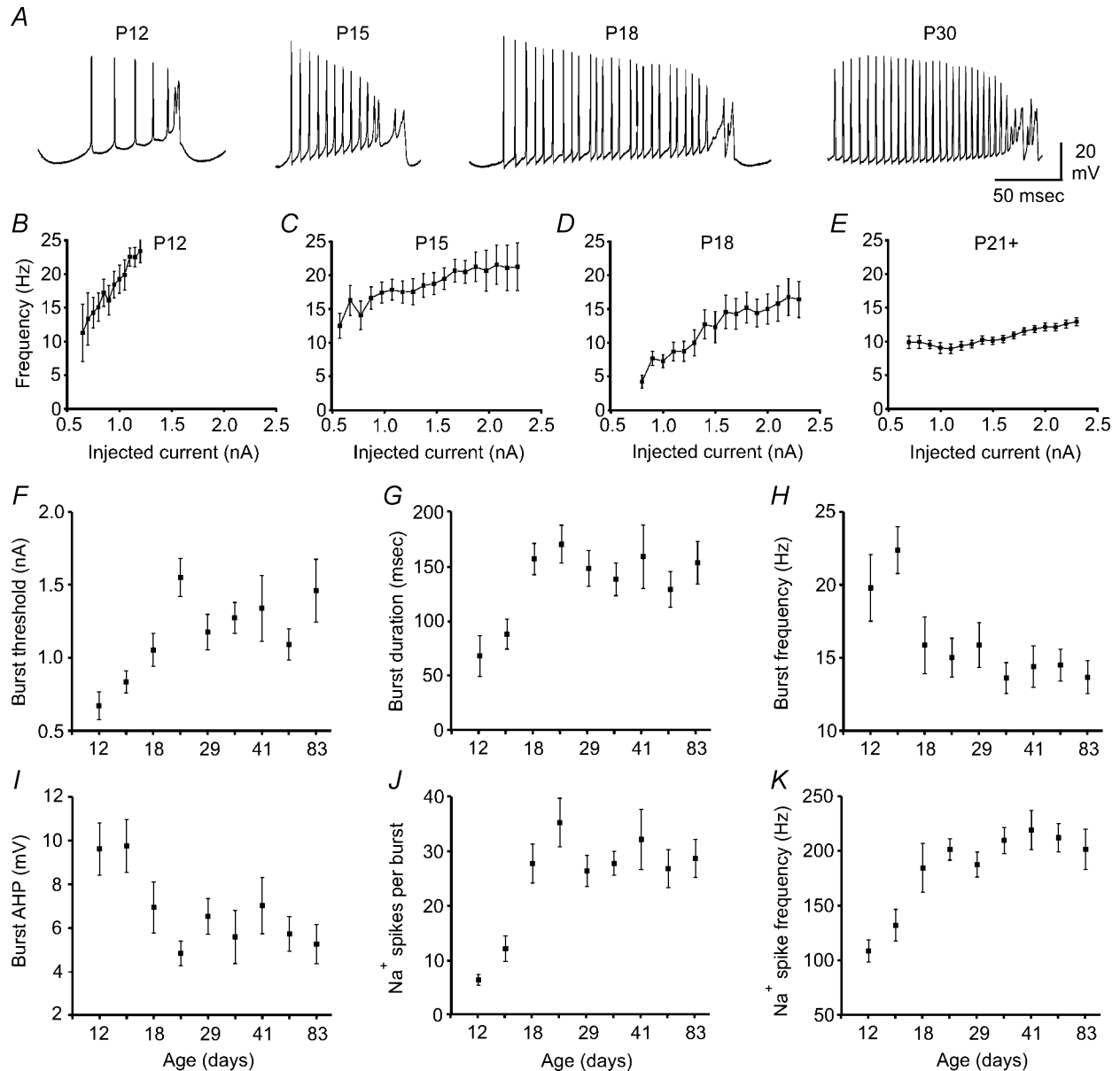


Figure 6. Characteristics of burst output maturation

A, Ca^{2+} - Na^+ burst output, first seen at P12, matured rapidly. B and C, the gain of the burst F - I relationship decreased between P12 (B) and P15 (C). D and E, by P18 the range of burst frequencies was increased (D) but matured to a nearly current-insensitive burst frequency response beyond \sim P21 (E). F, G, the current threshold to evoke bursting (F) and the duration of Ca^{2+} - Na^+ bursts (G) increased with age. H, I, the maximum frequency of Ca^{2+} - Na^+ burst output (H) and the amplitude of the burst AHP (I) decreased with age. J and K, the number of Na^+ spikes per Ca^{2+} - Na^+ burst increased with age (J), following a similar time course as the increase in Na^+ -spike frequency within each Ca^{2+} - Na^+ burst (K). Purkinje cells per data point: in B, 4-9; C, 5-16; D, 3-11; E, 5-70; F, 12-22; G, 12-23; H, 7-15; I, 12-22; J, 12-23; and K, 10-23.

hyperpolarized pause (Fig. 7A). The trimodal pattern is an intrinsic property of Purkinje cells as it is expressed by spontaneously behaving cells in the presence of synaptic blockers. The development of this pattern has been previously examined in mice. Here we extend these results to rats and consider the development over a greater age range.

We found that 228 of 268 (85%) of Purkinje cells at \geq P12 were spontaneously active. Of these, 99% displayed Ca^{2+} - Na^{+} bursts following stimulation. By comparison, 40 of 268 Purkinje cells at \geq P12 were quiet under spontaneous conditions, with an average resting membrane potential of -58 ± 1 mV. Ca^{2+} - Na^{+} bursts could not be evoked by intracellular current injection in any of these cells, although generation of a few Na^{+} spikes was possible. There were no differences in dendritic size between the spontaneously active and quiescent populations of cells. Thus, to obtain a true estimate of the proportion of Purkinje cells expressing the trimodal pattern as a function of age, spontaneously quiet cells were excluded from the analyses as they were incapable of generating one component of the trimodal pattern.

The proportion of Purkinje cells expressing the trimodal pattern changed as a function of age (Fig. 7B and Table 1). From P3 to P9 Purkinje cells spontaneously fired sustained low-frequency Na^{+} spikes with no evidence of a trimodal pattern (Fig. 7B and C). At P12 the trimodal pattern was present in 2 of 20 Purkinje cells, and by P24 was present in $> 80\%$ of spontaneously active cells (Fig. 7B and Table 1). Interestingly, the maturation of dendritic area (Fig. 1E) preceded and then paralleled the development of the trimodal pattern, as evidenced by the Boltzmann fits for these two variables (Fig. 7C). However, for any given age, there was no difference in dendritic area between those cells expressing the trimodal pattern and those that did not. These results suggest that additional factors that develop in concert with dendritic structure, presumably dendritic ion-channel expression, contribute to the developmental transition from a tonic Na^{+} -spike output mode to a trimodal output mode.

An age-dependent increase in the frequency of Na^{+} spikes during the tonic component of the trimodal pattern was noted (Fig. 7D and Table 1). At P18 the frequency of spontaneous Na^{+} -spike generation was significantly

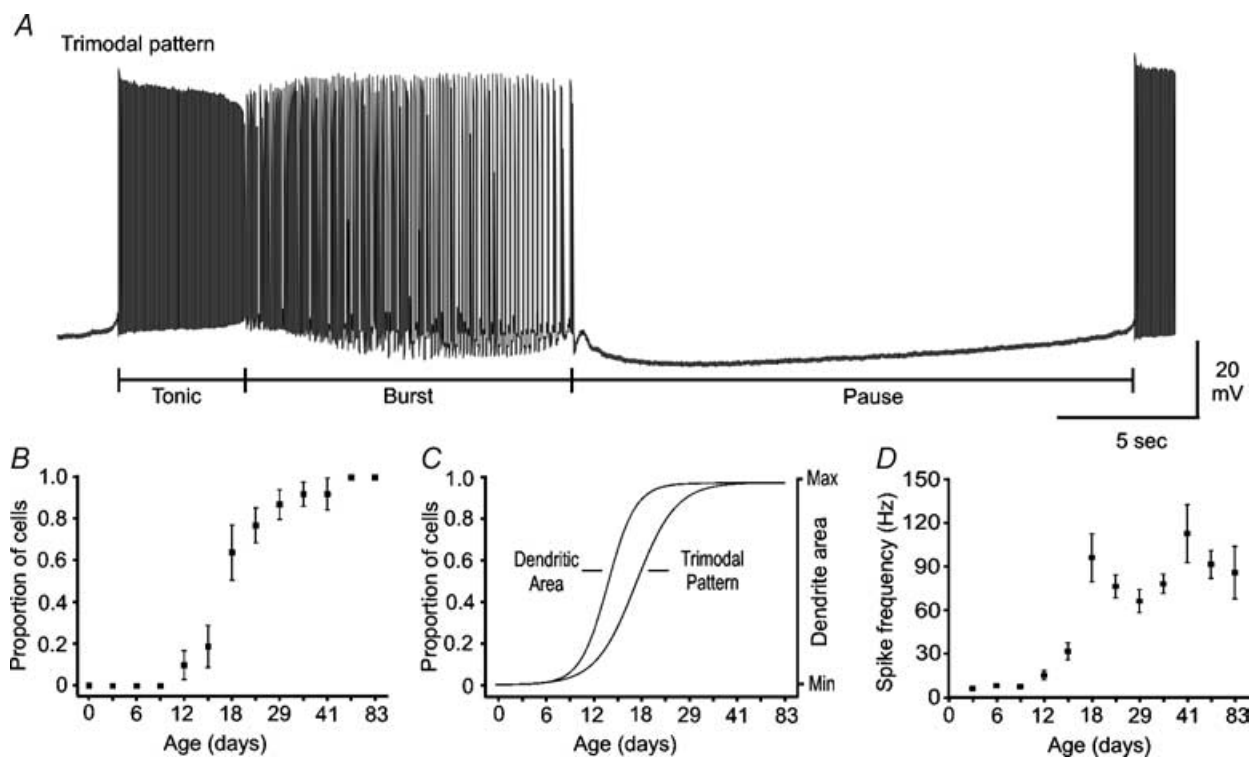


Figure 7. Developmental transition from tonic Na^{+} spiking to trimodal pattern

A, the trimodal pattern consists of a train of Na^{+} spikes, a series of Ca^{2+} - Na^{+} bursts and a hyperpolarizing pause. The pattern repeats continuously with little variability. B, the proportion of spontaneously active Purkinje cells expressing the trimodal pattern increased from zero prior to P12, to > 0.8 by P24. C, superimposing the Boltzmann fits of the development of the trimodal pattern (Fig. 7B) and dendritic area (Fig. 1E) revealed that dendritic growth preceded and then paralleled trimodal pattern expression. D, the mean frequency of Na^{+} spikes within the tonic component of the trimodal pattern increased substantially with age. Purkinje cells per data point in B and D, 9–25.

greater than at all lesser ages ($P < 0.01$); beyond P18 there were no additional changes in the frequency of spontaneous Na^+ -spike discharge. In contrast, there was no age-dependence for the duration of tonic Na^+ -spike discharge, the Ca^{2+} - Na^+ burst output, the pause, or the overall trimodal period (not shown). The mean durations of the trimodal components, averaged across all age groups (\geq P12), were: tonic 6.7 ± 0.7 s, Ca^{2+} - Na^+ burst 8.8 ± 0.4 s, pause 14.4 ± 0.5 s, and total pattern period 30.2 ± 1.0 s ($n \geq 108$ for each variable). We also found that the characteristics of the trimodal pattern were the same for both extracellular and whole-cell recordings (unpublished observations). Finally, the parameters of trimodal pattern output were equivalent for Purkinje cells sampled throughout the cerebellum.

Our results corroborate those from a previous study in mice; together they demonstrate that the trimodal pattern is a robust and normal output property of Purkinje cells, present in $> 80\%$ of cells at \geq P24 (Womack & Khodakhah, 2002a). Importantly, the trimodal pattern is also seen *in vivo* when climbing fibre transmission is blocked (Cerminara & Rawson, 2004). Our reported frequency of Na^+ -spike generation during the tonic component of trimodal discharge is similar to both the previous *in vitro* and *in vivo* reports. However, compared to our result of ~ 30 s, the overall period of previous measurements of the trimodal pattern was substantially longer, averaging ~ 5 min (mouse, *in vitro*) and ~ 1 min (rat, *in vivo*) (Womack & Khodakhah, 2002a; Cerminara & Rawson, 2004). To compare the developmental time course of the trimodal pattern in the rat to that in the mouse, we extracted the fraction of cells expressing the trimodal pattern from the plot in a previous report (Womack & Khodakhah, 2002a; their Fig. 3a). To this data we fit a Boltzmann function (Table 1) and found that the trimodal pattern in mouse matures ~ 4 days earlier than it does in rat. This is consistent with the observation that the mouse cerebellar cortex develops more rapidly than the rat (Altman, 1972). It is also interesting to note that the lack of a developmental change in the duration of the trimodal pattern, or any its constituent elements, contrasts with the progression of change found for Ca^{2+} - Na^+ -spike burst properties (Fig. 6). These data may thus suggest some differences in the underlying mechanisms for these two patterns, which were not further examined here.

Soma-dendritic properties

Dendritic and simultaneous soma-dendritic patch clamp recordings have contributed significantly to our understanding of Purkinje cell physiology (Stuart & Hausser, 1994; Roth & Hausser, 2001; Martina *et al.* 2003; McKay & Turner, 2004; Loewenstein *et al.* 2005). First, Na^+ action potentials are initiated at the first node of Ranvier, actively

backpropagate into the soma, and then decay rapidly in the proximal dendrites (Stuart & Hausser, 1994; McKay & Turner, 2004; Clark *et al.* 2005; Monsivais *et al.* 2005). The rapid decline in the amplitude of backpropagated Na^+ spikes is due to an exponential decrease in Na^+ -channel density with distance from the soma, and a steep rate of change in dendritic surface area with distance, due to the extensive branching pattern (Stuart & Hausser, 1994; Vetter *et al.* 2001). Second, the amplitudes of Ca^{2+} -mediated depolarizations, evoked by either intracellular current injection or climbing fibre stimulation, are significantly larger in dendrites than in somata (Stuart & Hausser, 1994; McKay & Turner, 2004).

Obtaining dual soma-dendrite recordings requires that continuous lengths of the soma-dendritic axis can be visualized. As this becomes difficult after the third postnatal week, our understanding of Purkinje cell soma-dendritic properties has been determined mostly from young animals. One important issue that emerges then is the degree of similarity in spike discharge between dendrites from young *vs.* older Purkinje cells. For the key Purkinje cell soma-dendritic properties identified above, we compared dual recordings from 17 young cells (P11 to P19, mean P15) and 4 adult cells (P23 to P90, mean P45). The distances between the somatic and dendritic electrodes were $54 \pm 8 \mu\text{m}$ and $70 \pm 10 \mu\text{m}$ for the young and old cells, respectively. We did not compare in detail the developmental stages of electrical activity at the dendritic level given the technical difficulty of obtaining dual recordings from older rats.

The results from a P14 cell (dendritic electrode at $90 \mu\text{m}$) and a P90 cell (dendritic electrode at $100 \mu\text{m}$) are reported in Fig. 8. In all cells examined, Na^+ spikes were recorded first in the soma and subsequently conducted with substantial decrement into the dendrites (Fig. 8A and B). As the distance between the somatic and dendritic recording electrodes increased, the amplitude of the dendritic Na^+ spikes progressively decreased for cells from both age groups. With sufficient distance, small amplitude Na^+ spikes occurring just prior to the termination of each Ca^{2+} - Na^+ burst were not measurable in the dendrites (Fig. 8C and D). We found that the Ca^{2+} spikes terminating Ca^{2+} - Na^+ bursts had substantially greater amplitudes in dendrites for both young and older cells (Fig. 8C and D). Compared to somatic Ca^{2+} spikes, the peak amplitudes of dendritic Ca^{2+} spikes were 11.0 ± 2.0 mV more depolarized for young cells, and 9.6 ± 3.1 mV more depolarized for older cells. Further, there was an exact correspondence between somatic and dendritic recordings for the numbers of Na^+ or Ca^{2+} spikes and for the total duration of Ca^{2+} - Na^+ bursts. This latter result substantiates the ability to assess the relative properties of spike discharge during development according to the nature of spike output detected at the soma. We did not consider the site of Ca^{2+} -spike initiation, as only two

measurement points per cell were insufficient to address this issue given the highly arborized dendritic structure of the Purkinje cell.

These comparisons suggest that somatic and dendritic spike properties unique to Purkinje cells, including a decremental backpropagation of Na⁺ spikes and large dendritic Ca²⁺ spikes, are expressed early in development. In fact, we found that these properties were evident in dual recordings even from P11 cells, which is only a few days after the onset of the extension of a single primary dendrite for many cells. These data thus indicate that the close correspondence between dendritic growth and Ca²⁺-dependent spike activity revealed in our developmental analysis reflects the appearance of prominent dendritic Ca²⁺ spikes. Moreover, an early expression of adult-like spike discharge patterns indicates that the influence of dendritic structure and ion-channel distribution on spike properties is established from the first period of dendritic extension in Purkinje cells. This comparison is also important in revealing that dual soma-dendrite whole-cell current clamp recordings

obtained from young animals can provide realistic insights into the workings of mature Purkinje cells.

Discussion

This study identified the maturation of electrophysiological properties of the cerebellar Purkinje cell, and by comparison to changes in dendritic structure, distinguished three morpho-physiological stages of development. During the first and last stages of development Purkinje cell physiology and anatomical structure were relatively stable. During the middle stage of development there were marked changes in cell output characteristics that occurred concomitant with a progressive increase in dendritic size and complexity. A previous modelling study in Purkinje cells highlighted dendritic geometry and ion-channel distribution within dendrites as key determinants of cell physiology (Vetter *et al.* 2001). The parallel timing of changes in input-output relations and dendritic growth identified in the present study confirms this important relationship. The

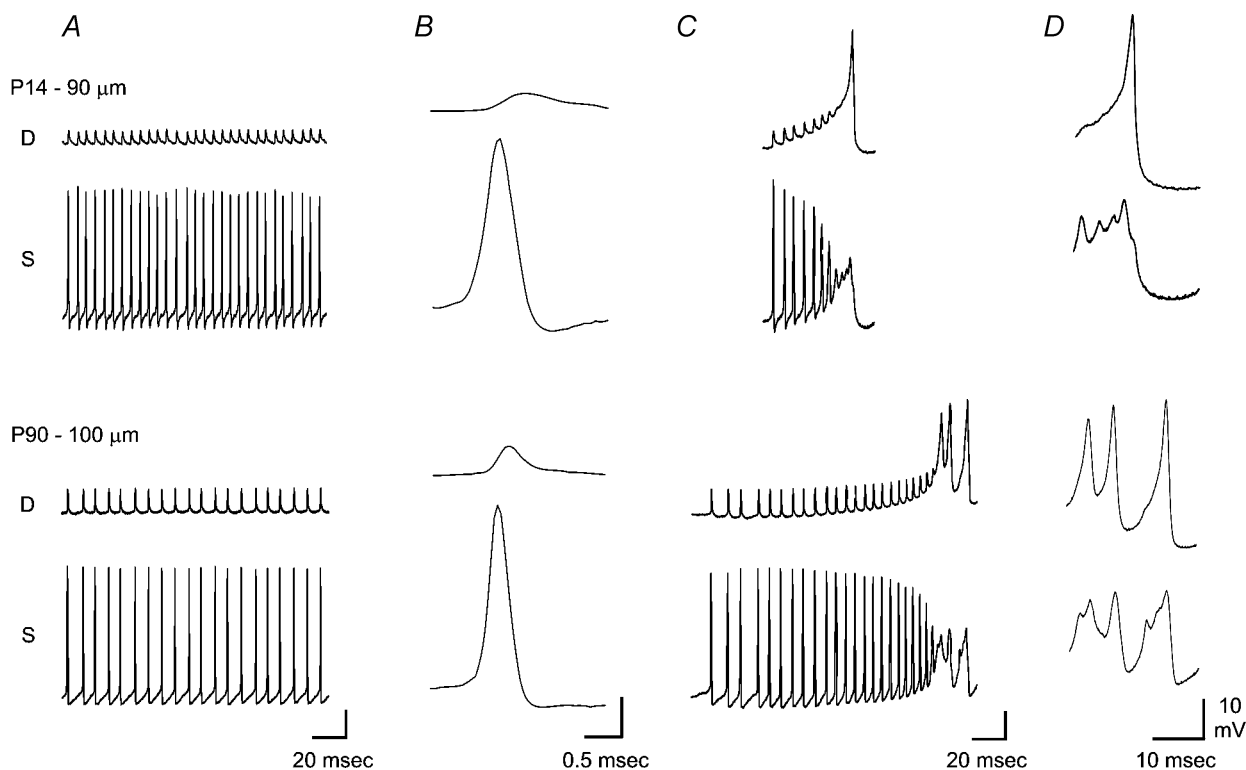


Figure 8. Soma-dendritic properties are similar for young and old Purkinje cells

Dual whole-cell soma (S) and dendrite (D) current clamp recordings for a Purkinje cell from a young rat (P14; 90 μm) and an old rat (P90; 100 μm). *A* and *B*, spontaneous Na⁺-spike discharge in the soma was faithfully reflected in the dendrites as backpropagated spikes of significantly diminished amplitude for both juvenile (top panels) and mature (bottom panels) cells. *B* shows expanded views of somatic and dendritic Na⁺ spikes shown in *A*. *C* and *D*, current-evoked depolarization at the soma resulted in the generation of Ca²⁺-Na⁺ bursts at both somatic and dendritic levels. The number of evoked spikes and the duration of each burst was always the same between the soma and the dendrite, although Ca²⁺-spike amplitude was always greater in the dendrites. *D* shows an expanded view of the burst-terminating Ca²⁺ spikes shown in *C*.

codevelopment of dendrites and Ca^{2+} -mediated spike discharge, as well as other developmental changes in Purkinje cell output, can be further correlated with the timing of expression of numerous ion channels along the soma-dendritic axis.

Na^+ channels

The Na^+ -spike waveform matured rapidly early in development. We observed a reduction in the voltage threshold for Na^+ -spike activation, and marked increases in peak rate of rise and net amplitude of the Na^+ spike over the first two stages of development (P3 to P18). These changes may reflect a developmental increase in the density of Na^+ -channel expression, a shift in the expression of specific Na^+ -channel α -subunits ($\text{Na}_v1.x$), or a change in Na^+ -channel kinetics due to β -subunit coexpression. Although changes in Na^+ -channel density or kinetics have not been examined in Purkinje cells, several lines of evidence point to a developmental regulation of the α -subunits $\text{Na}_v1.1$, $\text{Na}_v1.2$, $\text{Na}_v1.3$ and $\text{Na}_v1.6$, with complimentary expression of β -subunits (Oh *et al.* 1994; Felts *et al.* 1997; Levy-Mozziconacci *et al.* 1998; Schaller & Caldwell, 2000; Whitaker *et al.* 2000).

$\text{Na}_v1.1$ is not detected in Purkinje cells prenatally, but from P15 onwards there is evidence for somatic and perhaps dendritic labelling, whereas $\text{Na}_v1.2$ is present briefly around P2, with no evidence for adult expression (Westenbroek *et al.* 1989; Furuyama *et al.* 1993; Black *et al.* 1994; Felts *et al.* 1997; Vega-Saenz de Miera *et al.* 1997; Gong *et al.* 1999). $\text{Na}_v1.3$ is strongly expressed in putative Purkinje cells prenatally, with a diminished expression by P2 and little or no expression later in development (Furuyama *et al.* 1993; Black *et al.* 1994; Felts *et al.* 1997). Finally, $\text{Na}_v1.6$ is found across all developmental stages, with a somatic and prominent dendritic distribution (Felts *et al.* 1997; Caldwell *et al.* 2000; Schaller & Caldwell, 2000). The continuously high expression of $\text{Na}_v1.6$ is interesting, as this channel generates the resurgent Na^+ current which underlies the ability of Purkinje cells to fire repetitive Na^+ spikes (Raman & Bean, 1997; Raman *et al.* 1997; Khaliq *et al.* 2003; Grieco & Raman, 2004). These data suggest that $\text{Na}_v1.6$ α -subunits contribute to Purkinje cell output at all ages, and that $\text{Na}_v1.1$ α -subunits may contribute to the maturation of Na^+ -spike characteristics later in development.

Purkinje cells are further known to express both $\text{Na}_v\beta1$ and $\text{Na}_v\beta2$ -subunits (Oh *et al.* 1994; Levy-Mozziconacci *et al.* 1998; Whitaker *et al.* 2000), and by modifying the properties of the $\text{Na}_v1.1$ and $\text{Na}_v1.6$ α -subunits may contribute to the maturation of Na^+ -spike characteristics. For instance, Na^+ -channel β -subunits confer a hyperpolarizing shift in activation kinetics, an acceleration of activation and inactivation kinetics, and increase the density of α -subunit expression at the cell membrane

(Isom *et al.* 1994; Patton *et al.* 1994; Goldin, 1999). It is interesting that the modifications produced by β -subunit coexpression complement the developmental changes we measured in Na^+ -spike characteristics, including the leftward shift of spike activation voltage, the accelerated spike rise time, and increased spike amplitude. Although developmental regulation of β -subunit expression in Purkinje cells is unknown, it has been established that the expression of β -subunits in whole brain, increases during postnatal development (Gong *et al.* 1999), suggesting that the cerebellum may be similarly regulated.

Ca^{2+} channels

The transition from P3 to P12 from a single early and transient lower threshold Ca^{2+} spike to delayed and sustained higher threshold Ca^{2+} spikes suggests pronounced changes in the expression of Ca^{2+} -channel subtypes during Purkinje cell development. Purkinje cells from rat are known to express both low- and high-threshold Ca^{2+} channels throughout development (Kaneda *et al.* 1990; Nam & Hockberger, 1997). However, electrophysiological and immunohistochemical evidence suggest a change in the relative contributions of specific Ca^{2+} -channel subunits over time that matches the development of spike output properties reported here. During the first week of postnatal development, L-type Ca^{2+} channels show a prominent somatic expression and contribute > 60% of the Ca^{2+} influx to a Purkinje cell (Liljelund *et al.* 2000). At this age L-type channels underlie the low-threshold burst of spikes seen at the onset of depolarizing current injections (Liljelund *et al.* 2000). P/Q-, N- and R-type channels are also expressed, but make only a minor physiological contribution (Liljelund *et al.* 2000; Meacham *et al.* 2003). During the second week there is an increased expression of P/Q- and R-type channels, and by the end of this week, when Ca^{2+} - Na^+ bursts are first seen, P/Q-type Ca^{2+} channels are expressed prominently in the dendrites (Meacham *et al.* 2003). The expression level of P/Q-type channels remains high into adulthood, whereas there is a relative decrease in both L- and R-type channels (Mize *et al.* 2002; Meacham *et al.* 2003). Voltage clamp recordings confirm this shift in subunit dominance. By adulthood, ~90% of the total high-threshold Ca^{2+} current is conducted by P/Q-type channels, with L-type and N-type channels each contributing only ~5% (Regan, 1991; Mintz *et al.* 1992; Watanabe *et al.* 1998; Raman & Bean, 1999). The dominant high-threshold P/Q-type current contributes to the Ca^{2+} spike terminating each Ca^{2+} - Na^+ burst, and activates the large conductance Ca^{2+} -activated K^+ current implicated in the fast AHP of mature Na^+ spikes (Edgerton & Reinhart, 2003; Womack *et al.* 2004; Womack & Khodakhah, 2004).

Low-threshold T-type Ca^{2+} currents are also distributed across the soma-dendritic axis, and are present at all ages

(Crepel & Penit-Soria, 1986; Kaneda *et al.* 1990; Regan, 1991; Nam & Hockberger, 1997; McDonough & Bean, 1998; Craig *et al.* 1999; Raman & Bean, 1999; Talley *et al.* 1999; Swensen & Bean, 2003). In adult cells, T-type Ca^{2+} channels contribute some of the current underlying the rebound depolarization following anode break, and because of slowly deactivating tail currents produce a current flow between Na^+ spikes (Crepel & Penit-Soria, 1986; Swensen & Bean, 2003). However, given the strategies required to resolve the contribution of T-type currents to Purkinje cell output (Swensen & Bean, 2003) we are unable to specifically assign these channels to the developmental changes that we have reported.

Low threshold Ca^{2+} currents are particularly prominent in cultured Purkinje cells (Gruol *et al.* 1992; Mougnot *et al.* 1997; Pouille *et al.* 2000; Cavelier *et al.* 2002, 2003; Cavelier & Bossu, 2003). Interestingly, cultured Purkinje cells generate an output most similar to the P3 to P9/P12 Purkinje cells in the present study. This is particularly evident in the transient depolarization and burst of Na^+ spikes and the subsequent sustained low-frequency Na^+ -spike discharge that we see in young Purkinje cells from acute slices. This is the same pattern as the low-threshold complex spike and subsequent low-frequency Na^+ spikes that are observed in cultures (Gruol *et al.* 1992; Pouille *et al.* 2000; Cavelier & Bossu, 2003; Cavelier *et al.* 2003). Although the differences between Purkinje cells from acute adult slices and from mature cultures may be attributed in part to specific culture conditions (Bossu *et al.* 1989; Usowicz *et al.* 1992), our data suggest that the cultured Purkinje cell may be a faithful reflection of the early stage of physiological development. Further, we noticed that approximately one-half of our P12 Purkinje cells showed some dendritic development yet generated the immature spike output pattern, suggesting that within certain limits dendritic growth and ion-channel expression were insufficient to render a more mature physiology. This is correlated with the observation that cultured Purkinje cells have dendritic development, yet display a physiology consistent with an earlier developmental stage.

K^+ channels

Throughout the first few weeks of postnatal development Na^+ spikes became progressively narrower as the rate of spike repolarization increased. The Na^+ -spike AHP changed from a slowly activating and large-amplitude event to a fast activating, shallow amplitude and rapidly terminating event. The marked accommodation of Na^+ -spike frequency following the transient burst of Na^+ spikes disappeared after P12, and was replaced by Ca^{2+} - Na^+ burst output. Later, the burst AHPs underwent a gradual reduction in size. These changes cumulatively point to a significant developmental regulation of both

voltage-gated and Ca^{2+} -activated K^+ -channel function in Purkinje cells.

Purkinje cells express a wealth of voltage-gated K^+ channels. Immunohistochemical studies have identified the presence of members of the Kv1, Kv2, Kv3 and Kv4 families, as well as their associated accessory subunits (Drewe *et al.* 1992; Hwang *et al.* 1993; Goldman-Wohl *et al.* 1994; Weiser *et al.* 1994; Veh *et al.* 1995; Hugnot *et al.* 1996; Rhodes *et al.* 1996; Salinas *et al.* 1997; Tsaur *et al.* 1997; Serodio & Rudy, 1998; Martina *et al.* 2003; Xiong *et al.* 2004). The biophysical characterization and functional roles of the Kv1, Kv3 and Kv4 K^+ -channel families in Purkinje cells have been described (Sacco & Tempia, 2002; Martina *et al.* 2003; McKay & Turner, 2004; McKay *et al.* 2005). Of these, a developmental regulation of Kv3 channels would be most consistent with the changes in spike output properties observed in the present study. For instance, the narrowing of Na^+ spikes and the emergence of a fast AHP across development can be linked to a Kv3-mediated process, as Kv3 K^+ channels repolarize both somatic and dendritic Na^+ action potentials, and contribute to the generation of fast AHPs (Martina *et al.* 2003; McKay & Turner, 2004). Kv3 K^+ channels also repolarize dendritic Ca^{2+} spikes, thereby increasing the duration of Ca^{2+} - Na^+ bursts and the number of Na^+ spikes generated within each burst (McKay & Turner, 2004). The present work determined that both of these burst characteristics were regulated during development in a manner consistent with increased Kv3 expression. In support of this proposal, it has been shown that the Kv3.3-subunit is first expressed around P8, is found in all Purkinje cells by P12, and finally matures in the adult cerebellum (Goldman-Wohl *et al.* 1994).

The AHPs following Na^+ spikes and Ca^{2+} - Na^+ bursts are controlled by activation of both large conductance (BK) and small conductance (SK) Ca^{2+} -activated K^+ channels (Raman & Bean, 1999; Cingolani *et al.* 2002; Womack & Khodakhah, 2002b; Womack & Khodakhah, 2003, 2003; Khaliq *et al.* 2003; Swensen & Bean, 2003; McKay & Turner, 2004; Womack *et al.* 2004). Adult Purkinje cells express BK K^+ -channel α - and β -subunits in both somatic and proximal dendritic membranes (Knaus *et al.* 1996; Chang *et al.* 1997). Cultured Purkinje cells show a prominent increase in the expression of BK K^+ channels during the first few weeks of culture, whereas for Purkinje cells from acute slices, no differences in the effects of BK K^+ -channel blockers are observed between P13 and P31 (Muller & Yool, 1998; Edgerton & Reinhart, 2003). Together, these results suggest an early low expression of BK K^+ channels and attainment of adult-like levels late in the second week of development. Conversely, the expression of SK K^+ channels is high during the first two weeks of development, with a steady decline between P12 and P24 and low levels in the adult (Stocker & Pedarzani,

2000; Cingolani *et al.* 2002). Despite a lower expression, the functional role of SK K^+ channels in adult Purkinje cells is significant, contributing to the slow AHP following both Na^+ and Ca^{2+} spikes (Womack & Khodakhah, 2002a, 2003; Edgerton & Reinhart, 2003; McKay & Turner, 2004). A developmental increase in BK expression and decrease in SK expression is consistent with our findings of a transition from slow AHPs to fast AHPs, and also a marked increase in Na^+ -spike frequency.

Implications for cerebellar function

The developmental change in the ability to generate Ca^{2+} - Na^+ bursts and dendritic Ca^{2+} spikes is expected to alter soma-dendritic information processing in an age-dependent manner. An age-dependent change in soma-axonic processing is also expected. For instance, we found that Na^+ -spike generation in mature Purkinje cells could exceed 200 Hz. However, transmission of Na^+ spikes down Purkinje cell axons is not completely faithful beyond this frequency (Khaliq & Raman, 2005; Monsivais *et al.* 2005). Thus, high-frequency Na^+ -spike generation confers an age-dependent change in information processing between somatic and axonal compartments.

Additionally, we have shown that the characteristics of rebound discharge in deep cerebellar nuclear (DCN) neurones are determined by the frequency of Purkinje cell discharge (McKay *et al.* 2005). For these experiments we used tonic or bursting Purkinje cell outputs as extracellular stimulation protocols to activate inhibitory Purkinje cell axons synapsing on DCN neurones. We found that low-frequency (~ 60 Hz) stimulation resulted in short latency and high-frequency rebound discharges of Na^+ spikes in DCN neurones, whereas higher frequency (~ 150 Hz) stimulation resulted in longer latency and lower frequency rebound discharges (McKay *et al.* 2005). The frequency dependence of rebound discharge characteristics occurred irrespectively of whether the stimuli were grouped as a tonic train of inputs, or as a series of burst inputs. The transition towards higher frequency Na^+ -spike discharge began at $\sim P12$, which coincides with the attainment of adult-like GABA receptor immunoreactivity on the DCN neurones (Garin & Escher, 2001). Therefore the increase in the frequency range of Na^+ -spike output during development should be reflected in Purkinje cell control over DCN neurones by influencing the characteristics of rebound discharge.

Maturation of cerebellar-controlled behaviours

The Purkinje cell provides the only output of the cerebellar cortex, and the only output of the entire vestibulocerebellum. Thus, one prediction is that the

maturation of Purkinje cell electrophysiology should correspond to the maturation of cerebellar-dependent behaviours. In fact, inspection of the time courses of several behaviours known to depend on cerebellar control, including postural control, balance control, general locomotor activity, and coordination of limb position, all reveal a marked increase in proficiency from late in the second week to the third week of postnatal development (Altman & Bayer, 1997). The cerebellum further contains the neural substrates underlying the learning of the conditioned eye-blink response (Steinmetz, 2000; Christian & Thompson, 2003). Maturation of the eye-blink response occurs between P17 and P24, and the rate of conditioning increases roughly linearly over this age range (Stanton *et al.* 1998). The maturation of this response is accompanied by an increase in the number of Purkinje cells recruited into the behaviour, as well as a change in the timing of Purkinje cell discharge, such that Purkinje cell discharge occurs at a more consistent interval preceding the onset of the unconditional stimulus (Nicholson & Freeman, 2004).

From our data, postural and motor behaviours begin to mature at the time when Purkinje cells begin marked dendritic growth and move away from immature input-output relations. However, learning behaviours do not materialize until the Purkinje cell dendrite is already well established, and the input-output relations are essentially fully mature. These results suggest that some motor and postural behaviours may be sustained by a certain minimal amount of Purkinje cell and cerebellar development, whereas the complexities of associative learning are correlated with more sophisticated development. In this regard, it is interesting that dendritic geometry continues to change for almost 2 months beyond the last major changes in cell output. This observation suggests that final development of distal dendrites may contribute to subtle fine-tuning of cell output that is below the resolution of behavioural or patch clamp techniques, or that development shifts more to refining aspects of synaptic plasticity and learning capacity not examined here.

References

- Addison WHF (1911). The development of the Purkinje cells and of the cortical layers in the cerebellum of the albino rat. *J Comp Neurol* **21**, 459–487.
- Altman J (1969). Autoradiographic and histological studies of postnatal neurogenesis. 3. Dating the time of production and onset of differentiation of cerebellar microneurons in rats. *J Comp Neurol* **136**, 269–293.
- Altman J (1972). Postnatal development of the cerebellar cortex in the rat. II. Phases in the maturation of Purkinje cells and of the molecular layer. *J Comp Neurol* **145**, 399–463.
- Altman J & Bayer SA (1997). *Development of the Cerebellar System*. CRC Press, New York.

- Black JA, Yokoyama S, Higashida H, Ransom BR & Waxman SG (1994). Sodium channel mRNAs I, II and III in the CNS: cell-specific expression. *Brain Res Mol Brain Res* **22**, 275–289.
- Bossu JL, Dupont JL & Feltz A (1989). Calcium currents in rat cerebellar Purkinje cells maintained in culture. *Neuroscience* **30**, 605–617.
- Caldwell JH, Schaller KL, Lasher RS, Peles E & Levinson SR (2000). Sodium channel Na_v1.6 is localized at nodes of ranvier, dendrites, and synapses. *Proc Natl Acad Sci USA* **97**, 5616–5620.
- Cavelier P & Bossu JL (2003). Dendritic low-threshold Ca²⁺ channels in rat cerebellar Purkinje cells: possible physiological implications. *Cerebellum* **2**, 196–205.
- Cavelier P, Desplantez T, Beekenkamp H & Bossu JL (2003). K⁺ channel activation and low-threshold Ca²⁺ spike of rat cerebellar Purkinje cells *in vitro*. *Neuroreport* **14**, 167–171.
- Cavelier P, Pouille F, Desplantez T, Beekenkamp H & Bossu JL (2002). Control of the propagation of dendritic low-threshold Ca²⁺ spikes in Purkinje cells from rat cerebellar slice cultures. *J Physiol* **540**, 57–72.
- Cerminara NL & Rawson JA (2004). Evidence that climbing fibers control an intrinsic spike generator in cerebellar Purkinje cells. *J Neurosci* **24**, 4510–4517.
- Chang CP, Dworetzky SI, Wang J & Goldstein ME (1997). Differential expression of the alpha and beta subunits of the large-conductance calcium-activated potassium channel: implication for channel diversity. *Brain Res Mol Brain Res* **45**, 33–40.
- Christian KM & Thompson RF (2003). Neural substrates of eyeblink conditioning: acquisition and retention. *Learn Mem* **10**, 427–455.
- Cingolani LA, Gymnopoulos M, Boccaccio A, Stocker M & Pedarzani P (2002). Developmental regulation of small-conductance Ca²⁺-activated K⁺ channel expression and function in rat Purkinje neurons. *J Neurosci* **22**, 4456–4467.
- Clark BA, Monsivais P, Branco T, London M & Hausser M (2005). The site of action potential initiation in cerebellar Purkinje neurons. *Nat Neurosci* **8**, 137–139.
- Craig PJ, Beattie RE, Folly EA, Banerjee MD, Reeves MB, Priestley JV, Carney SL, Sher E, Perez-Reyes E & Volsen SG (1999). Distribution of the voltage-dependent calcium channel alpha1G subunit mRNA and protein throughout the mature rat brain. *Eur J Neurosci* **11**, 2949–2964.
- Crepel F (1971). Maturation of climbing fiber responses in the rat. *Brain Res* **35**, 272–276.
- Crepel F (1972). Maturation of the cerebellar Purkinje cells I. Postnatal evolution of the Purkinje cell spontaneous firing in the rat. *Exp Brain Res* **14**, 463–471.
- Crepel F (1974). Excitatory and inhibitory processes acting upon cerebellar Purkinje cells during maturation in the rat; influence of hypothyroidism. *Exp Brain Res* **20**, 403–420.
- Crepel F & Penit-Soria J (1986). Inward rectification and low threshold calcium conductance in rat cerebellar Purkinje cells. An *in vitro* study. *J Physiol* **372**, 1–23.
- Drewe JA, Verma S, Frech G & Joho RH (1992). Distinct spatial and temporal expression patterns of K⁺ channel mRNAs from different subfamilies. *J Neurosci* **12**, 538–548.
- Edgerton JR & Reinhart PH (2003). Distinct contributions of small and large conductance Ca²⁺-activated K⁺ channels to rat Purkinje neuron function. *J Physiol* **548**, 53–69.
- Felts PA, Yokoyama S, Dib-Hajj S, Black JA & Waxman SG (1997). Sodium channel alpha-subunit mRNAs I, II, III, NaG, Na6 and hNE (PN1): different expression patterns in developing rat nervous system. *Brain Res Mol Brain Res* **45**, 71–82.
- Furuyama T, Morita Y, Inagaki S & Takagi H (1993). Distribution of I, II and III subtypes of voltage-sensitive Na⁺ channel mRNA in the rat brain. *Brain Res Mol Brain Res* **17**, 169–173.
- Garin N & Escher G (2001). The development of inhibitory synaptic specializations in the mouse deep cerebellar nuclei. *Neuroscience* **105**, 431–441.
- Goldin AL (1999). Diversity of mammalian voltage-gated sodium channels. *Ann N Y Acad Sci* **868**, 38–50.
- Goldman-Wohl DS, Chan E, Baird D & Heintz N (1994). Kv3.3b: a novel Shaw type potassium channel expressed in terminally differentiated cerebellar Purkinje cells and deep cerebellar nuclei. *J Neurosci* **14**, 511–522.
- Gong B, Rhodes KJ, Bekele-Arcuri Z & Trimmer JS (1999). Type I and type II Na⁺ channel alpha-subunit polypeptides exhibit distinct spatial and temporal patterning, and association with auxiliary subunits in rat brain. *J Comp Neurol* **412**, 342–352.
- Goodlett CR, Hamre KM & West JR (1990). Regional differences in the timing of dendritic outgrowth of Purkinje cells in the vermal cerebellum demonstrated by MAP2 immunocytochemistry. *Brain Res Dev Brain Res* **53**, 131–134.
- Grieco TM & Raman IM (2004). Production of resurgent current in NaV1.6-null Purkinje neurons by slowing sodium channel inactivation with beta-pompilidotoxin. *J Neurosci* **24**, 35–42.
- Gruol DL, Deal CR & Yool AJ (1992). Developmental changes in calcium conductances contribute to the physiological maturation of cerebellar Purkinje neurons in culture. *J Neurosci* **12**, 2838–2848.
- Gruol DL & Franklin CL (1987). Morphological and physiological differentiation of Purkinje neurons in cultures of rat cerebellum. *J Neurosci* **7**, 1271–1293.
- Hausser M & Clark BA (1997). Tonic synaptic inhibition modulates neuronal output pattern and spatiotemporal synaptic integration. *Neuron* **19**, 665–678.
- Hockberger PE, Tseng HY & Connor JA (1989). Development of rat cerebellar Purkinje cells: electrophysiological properties following acute isolation and in long-term culture. *J Neurosci* **9**, 2258–2271.
- Hugnot JP, Salinas M, Lesage F, Guillemare E, de Weille J, Heurteaux C, Mattei MG & Lazdunski M (1996). Kv8.1, a new neuronal potassium channel subunit with specific inhibitory properties towards Shab and Shaw channels. *EMBO J* **15**, 3322–3331.
- Hwang PM, Fotuhi M, Bredt DS, Cunningham AM & Snyder SH (1993). Contrasting immunohistochemical localizations in rat brain of two novel K⁺ channels of the Shab subfamily. *J Neurosci* **13**, 1569–1576.
- Isom LL, De Jongh KS & Catterall WA (1994). Auxiliary subunits of voltage-gated ion channels. *Neuron* **12**, 1183–1194.

- Ito M (1984). *The Cerebellum and Neural Control*. Raven, New York.
- M, Wakamori M, Ito C & Akaike N (1990a). Low-threshold calcium current in isolated Purkinje cell bodies of rat cerebellum. *J Neurophysiol* **63**, 1046–1051.
- Kaneda M, Wakamori M, Ito C & Akaike N (1990). Low-threshold calcium current in isolated Purkinje cell bodies of rat cerebellum. *J Neurophysiol* **63**, 1046–1051.
- Khalik ZM, Gouwens NW & Raman IM (2003). The contribution of resurgent sodium current to high-frequency firing in Purkinje neurons: an experimental and modeling study. *J Neurosci* **23**, 4899–4912.
- Khalik ZM & Raman IM (2005). Axonal propagation of simple and complex spikes in cerebellar Purkinje neurons. *J Neurosci* **25**, 454–463.
- Knaus HG, Schwarzer C, Koch RO, Eberhart A, Kaczorowski GJ, Glossmann H, Wunder F, Pongs O, Garcia ML & Sperk G (1996). Distribution of high-conductance Ca^{2+} -activated K^{+} channels in rat brain: targeting to axons and nerve terminals. *J Neurosci* **16**, 955–963.
- Levy-Mozziconacci A, Alcaraz G, Giraud P, Boudier JA, Caillol G, Couraud F & Autillo-Touati A (1998). Expression of the mRNA for the beta 2 subunit of the voltage-dependent sodium channel in rat CNS. *Eur J Neurosci* **10**, 2757–2767.
- Liljelund P, Netzeband JG & Gruol DL (2000). L-type calcium channels mediate calcium oscillations in early postnatal Purkinje neurons. *J Neurosci* **20**, 7394–7403.
- Llinas R & Sugimori M (1980a). Electrophysiological properties of *in vitro* Purkinje cell somata in mammalian cerebellar slices. *J Physiol* **305**, 171–195.
- Llinas R & Sugimori M (1980b). Electrophysiological properties of *in vitro* Purkinje cell dendrites in mammalian cerebellar slices. *J Physiol* **305**, 197–213.
- Loewenstein Y, Mahon S, Chadderton P, Kitamura K, Sompolinsky H, Yarom Y & Hausser M (2005). Bistability of cerebellar Purkinje cells modulated by sensory stimulation. *Nat Neurosci* **8**, 202–211.
- Martina M, Yao GL & Bean BP (2003). Properties and functional role of voltage-dependent potassium channels in dendrites of rat cerebellar Purkinje neurons. *J Neurosci* **23**, 5698–5707.
- McDonough SI & Bean BP (1998). Mibefradil inhibition of T-type calcium channels in cerebellar Purkinje neurons. *Mol Pharmacol* **54**, 1080–1087.
- McKay BE, Molineux ML, Mehaffey WH & Turner RW (2005). $\text{Kv}1$ K^{+} channels control Purkinje cell output to facilitate postsynaptic rebound discharge in deep cerebellar neurons. *J Neurosci* **25**, 1481–1492.
- McKay BE & Turner RW (2004). $\text{Kv}3$ K^{+} channels enable burst output in rat cerebellar Purkinje cells. *Eur J Neurosci* **20**, 729–739.
- Meacham CA, White LD, Barone S Jr & Shafer TJ (2003). Ontogeny of voltage-sensitive calcium channel α_{1A} and α_{1E} subunit expression and synaptic function in rat central nervous system. *Brain Res Dev Brain Res* **142**, 47–65.
- Mintz IM, Adams ME & Bean BP (1992). P-type calcium channels in rat central and peripheral neurons. *Neuron* **9**, 85–95.
- Mize RR, Graham SK & Cork RJ (2002). Expression of the L-type calcium channel in the developing mouse visual system by use of immunocytochemistry. *Brain Res Dev Brain Res* **136**, 185–195.
- Monsivais P, Clark BA, Roth A & Hausser M (2005). Determinants of action potential propagation in cerebellar Purkinje cell axons. *J Neurosci* **25**, 464–472.
- Mouginot D, Bossu JL & Gahwiler BH (1997). Low-threshold Ca^{2+} currents in dendritic recordings from Purkinje cells in rat cerebellar slice cultures. *J Neurosci* **17**, 160–170.
- Muller YL & Yool AJ (1998). Increased calcium-dependent K^{+} channel activity contributes to the maturation of cellular firing patterns in developing cerebellar Purkinje neurons. *Brain Res Dev Brain Res* **108**, 193–203.
- Nam SC & Hockberger PE (1997). Analysis of spontaneous electrical activity in cerebellar Purkinje cells acutely isolated from postnatal rats. *J Neurobiol* **33**, 18–32.
- Nicholson DA & Freeman JH Jr (2004). Developmental changes in eyeblink conditioning and simple spike activity in the cerebellar cortex. *Dev Psychobiol* **44**, 45–57.
- Oh Y, Sashihara S & Waxman SG (1994). In situ hybridization localization of the Na^{+} channel beta 1 subunit mRNA in rat CNS neurons. *Neurosci Lett* **176**, 119–122.
- Patton DE, Isom LL, Catterall WA & Goldin AL (1994). The adult rat brain beta 1 subunit modifies activation and inactivation gating of multiple sodium channel alpha subunits. *J Biol Chem* **269**, 17649–17655.
- Pouille F, Cavelier P, Desplantez T, Beekenkamp H, Craig PJ, Beattie RE, Volsen SG & Bossu JL (2000). Dendro-somatic distribution of calcium-mediated electrogenesis in Purkinje cells from rat cerebellar slice cultures. *J Physiol* **527**, 265–282.
- Puro DG & Woodward DJ (1977a). Maturation of evoked climbing fiber input to rat cerebellar Purkinje cells (I.). *Exp Brain Res* **28**, 85–100.
- Puro DG & Woodward DJ (1977b). Maturation of evoked mossy fiber input to rat cerebellar Purkinje cells (II.). *Exp Brain Res* **28**, 427–441.
- Raman IM & Bean BP (1997). Resurgent sodium current and action potential formation in dissociated cerebellar Purkinje neurons. *J Neurosci* **17**, 4517–4526.
- Raman IM & Bean BP (1999). Ionic currents underlying spontaneous action potentials in isolated cerebellar Purkinje neurons. *J Neurosci* **19**, 1663–1674.
- Raman IM, Sprunger LK, Meisler MH & Bean BP (1997). Altered subthreshold sodium currents and disrupted firing patterns in Purkinje neurons of *Scn8a* mutant mice. *Neuron* **19**, 881–891.
- Regan LJ (1991). Voltage-dependent calcium currents in Purkinje cells from rat cerebellar vermis. *J Neurosci* **11**, 2259–2269.
- Rhodes KJ, Monaghan MM, Barrezueta NX, Nawoschik S, Bekele-Arcuri Z, Matos MF, Nakahira K, Schechter LE & Trimmer JS (1996). Voltage-gated K^{+} channel beta subunits: expression and distribution of Kv beta 1 and Kv beta 2 in adult rat brain. *J Neurosci* **16**, 4846–4860.
- Roth A & Hausser M (2001). Compartmental models of rat cerebellar Purkinje cells based on simultaneous somatic and dendritic patch-clamp recordings. *J Physiol* **535**, 445–472.

- Sacco T & Tempia F (2002). A-type potassium currents active at subthreshold potentials in mouse cerebellar Purkinje cells. *J Physiol* **543**, 505–520.
- Salinas M, Duprat F, Heurteaux C, Hugnot JP & Lazdunski M (1997). New modulatory alpha subunits for mammalian Shab K⁺ channels. *J Biol Chem* **272**, 24371–24379.
- Schaller KL & Caldwell JH (2000). Developmental and regional expression of sodium channel isoform NaCh6 in the rat central nervous system. *J Comp Neurol* **420**, 84–97.
- Serodio P & Rudy B (1998). Differential expression of Kv4 K⁺ channel subunits mediating subthreshold transient K⁺ (A-type) currents in rat brain. *J Neurophysiol* **79**, 1081–1091.
- Stanton ME, Fox GD & Carter CS (1998). Ontogeny of the conditioned eyeblink response in rats: acquisition or expression? *Neuropharmacology* **37**, 623–632.
- Steinmetz JE (2000). Brain substrates of classical eyeblink conditioning: a highly localized but also distributed system. *Behav Brain Res* **110**, 13–24.
- Stocker M & Pedarzani P (2000). Differential distribution of three Ca²⁺-activated K⁺ channel subunits, SK1, SK2, and SK3, in the adult rat central nervous system. *Mol Cell Neurosci* **15**, 476–493.
- Stuart GJ, Dodt HU & Sakmann B (1993). Patch-clamp recordings from the soma and dendrites of neurons in brain slices using infrared video microscopy. *Pflugers Arch* **423**, 511–518.
- Stuart G & Hausser M (1994). Initiation and spread of sodium action potentials in cerebellar Purkinje cells. *Neuron* **13**, 703–712.
- Swensen AM & Bean BP (2003). Ionic mechanisms of burst firing in dissociated Purkinje neurons. *J Neurosci* **23**, 9650–9663.
- Talley EM, Cribbs LL, Lee JH, Daud A, Perez-Reyes E & Bayliss DA (1999). Differential distribution of three members of a gene family encoding low voltage-activated (T-type) calcium channels. *J Neurosci* **19**, 1895–1911.
- Tank DW, Sugimori M, Connor JA & Llinas RR (1988). Spatially resolved calcium dynamics of mammalian Purkinje cells in cerebellar slice. *Science* **242**, 773–777.
- Telgkamp P, Padgett DE, Ledoux VA, Woolley CS & Raman IM (2004). Maintenance of high-frequency transmission at Purkinje to cerebellar nuclear synapses by spillover from boutons with multiple release sites. *Neuron* **41**, 113–126.
- Tsaur ML, Chou CC, Shih YH & Wang HL (1997). Cloning, expression and CNS distribution of Kv4.3, an A-type K⁺ channel alpha subunit. *FEBS Lett* **400**, 215–220.
- Usowicz MM, Sugimori M, Cherksey B & Llinas R (1992). P-type calcium channels in the somata and dendrites of adult cerebellar Purkinje cells. *Neuron* **9**, 1185–1199.
- Vega-Saenz de Miera EC, Rudy B, Sugimori M & Llinas R (1997). Molecular characterization of the sodium channel subunits expressed in mammalian cerebellar Purkinje cells. *Proc Natl Acad Sci U S A* **94**, 7059–7064.
- Veh RW, Lichtinghagen R, Sewing S, Wunder F, Grumbach IM & Pongs O (1995). Immunohistochemical localization of five members of the Kv1 channel subunits: contrasting subcellular locations and neuron-specific co-localizations in rat brain. *Eur J Neurosci* **7**, 2189–2205.
- Vetter P, Roth A & Hausser M (2001). Propagation of action potentials in dendrites depends on dendritic morphology. *J Neurophysiol* **85**, 926–937.
- Watanabe S, Takagi H, Miyasho T, Inoue M, Kirino Y, Kudo Y & Miyakawa H (1998). Differential roles of two types of voltage-gated Ca²⁺ channels in the dendrites of rat cerebellar Purkinje neurons. *Brain Res* **791**, 43–55.
- Weiser M, Vega-Saenz de Miera E, Kentros C, Moreno H, Franzen L, Hillman D, Baker H & Rudy B (1994). Differential expression of Shaw-related K⁺ channels in the rat central nervous system. *J Neurosci* **14**, 949–972.
- Westenbroek RE, Merrick DK & Catterall WA (1989). Differential subcellular localization of the RI and RII Na⁺ channel subtypes in central neurons. *Neuron* **3**, 695–704.
- Whitaker WR, Clare JJ, Powell AJ, Chen YH, Faull RL & Emson PC (2000). Distribution of voltage-gated sodium channel alpha-subunit and beta-subunit mRNAs in human hippocampal formation, cortex, and cerebellum. *J Comp Neurol* **422**, 123–139.
- Womack MD, Chevez C & Khodakhah K (2004). Calcium-activated potassium channels are selectively coupled to P/Q-type calcium channels in cerebellar Purkinje neurons. *J Neurosci* **24**, 8818–8822.
- Womack M & Khodakhah K (2002a). Active contribution of dendrites to the tonic and trimodal patterns of activity in cerebellar Purkinje neurons. *J Neurosci* **22**, 10603–10612.
- Womack MD & Khodakhah K (2002b). Characterization of large conductance Ca²⁺-activated K⁺ channels in cerebellar Purkinje neurons. *Eur J Neurosci* **16**, 1214–1222.
- Womack MD & Khodakhah K (2003). Somatic and dendritic small-conductance calcium-activated potassium channels regulate the output of cerebellar Purkinje neurons. *J Neurosci* **23**, 2600–2607.
- Womack MD & Khodakhah K (2004). Dendritic control of spontaneous bursting in cerebellar Purkinje cells. *J Neurosci* **24**, 3511–3521.
- Woodward DJ, Hoffer BJ & Lapham LW (1969). Postnatal development of electrical and enzyme histochemical activity in Purkinje cells. *Exp Neurol* **23**, 120–139.
- Xiong H, Kovacs I & Zhang Z (2004). Differential distribution of KChIPs mRNAs in adult mouse brain. *Brain Res Mol Brain Res* **128**, 103–111.

Acknowledgements

This work was funded by the Canadian Institutes for Health Research. R.W.T. is an Alberta Heritage Foundation for Medical Research Scientist. B.E.M. is supported by a Canada Graduate Scholarship from the Canadian Institutes for Health Research, a Killam Trust scholarship, and a Steinhauer Doctoral Award. The authors wish to thank M. Kruskic for expert technical assistance and W.H. Mehaffey for helpful discussions.